Combustion and Flame xxx (xxxx) xxx

Contents lists available at ScienceDirect

Combustion and Flame

journal homepage: www.elsevier.com/locate/combustflame

A detailed kinetic model for aromatics formation from small hydrocarbon and gasoline surrogate fuel combustion

Raymond Langer, Qian Mao*, Heinz Pitsch

Institute for Combustion Technology, RWTH Aachen University, Aachen 52056, Germany

ARTICLE INFO

Article history:
Received 16 June 2022
Revised 25 November 2022
Accepted 4 December 2022
Available online xxx

Keywords:
PAH
Chemical kinetic modeling
Reaction flux analysis

ABSTRACT

This work develops a detailed chemical kinetic model for Polycyclic Aromatic Hydrocarbon (PAH) chemistry that builds on a chemical model for gasoline surrogates by Cai et al. [Proc. Combust. Inst. 37 (2019) 639–647]. Informed by ab-initio and experimental studies, the model development emphasizes the prediction of soot precursors starting from C_3H_4 isomers up to the size of acepyrene. The proposed model was validated against experimental measurements from 79 publications, including ignition delay times, laminar burning velocities, and speciation data for several fuels in various conditions. A validation against measured peak mole fractions from 31 counterflow flames demonstrates an average prediction error of aromatic species up to the size of acenaphthalene below a factor of three. Additionally, the effects of experimental uncertainty are quantitatively discussed by computing confidence intervals for the true model prediction error. The formation of two-ring aromatic species is often still considered poorly understood. Accordingly, special attention is given to the formation of indene and naphthalene. Reaction flux analyses based on rigorously defined species selection criteria reveal that indene formation pathways are initiated by reactions of phenyl and benzyl and described by the reaction kinetics from theoretical calculations. In contrast, naphthalene formation is dominated by more uncertain pathways relying on estimated rates that are initiated by reactions of benzene and fulvenallenyl. Five-member rings on the periphery of PAH species and soot particles play a crucial role in recent experimental and theoretical studies. Therefore, this work investigates acenaphthene and other $C_{12}H_8$ isomers. The most abundant $C_{12}H_8$ isomers are acenaphthene, 1-ethynylnaphthalene, and 2-ethynylnaphthalene, and their respective concentrations are predicted to be similar in many flames. Furthermore, reaction flux analyses show that their formation is dominated by HACA routes starting from naphthalene.

© 2022 The Authors. Published by Elsevier Inc. on behalf of The Combustion Institute.
This is an open access article under the CC BY license (http://creativecommons.org/licenses/by/4.0/)

1. Introduction

Soot is a pollutant produced during the incomplete combustion of hydrocarbon fuels. Its negative impacts on human health [1,2], process efficiency [3], and global warming [4–6] are well known. One significant source of soot particle emissions is the combustion of diesel, gasoline, or kerosene fuels in engines. As tighter engine regulations enforcing reduced soot emissions are expected to mitigate harmful effects on climate and human health [6,7], pressure to design cleaner combustion engines increased. Computational fluid dynamics calculations are often applied in engine design, which motivates the development of predictive models for soot formation and soot particle properties.

Modeling soot formation from the combustion of hydrocarbon fuels requires predictions of several species' concentrations from a detailed chemical kinetic model [8–13]. Accumulating theoretical and experimental evidence suggests that polycyclic aromatic hydrocarbon (PAH) species play a major role in soot formation [14]. As a result, several kinetic models have been developed for PAH growth [8,15–34]. Still, reliable and accurate reaction rate coefficient data of several key elementary chemical reactions involved in these processes have only recently become available, especially for the broad range of temperatures and pressures relevant to combustion conditions.

While the formation of the simplest aromatic species, benzene, is considered well understood by recent chemical kinetic and soot modeling studies [10,35–37], the formation chemistry of two- and three-ring aromatic species remains, in part, unclear [36]. The quantitative analysis of Dong et al. [37] substantiates the qualitative assessment of Hansen et al. [36]. Dong et al. [37] developed a detailed surrogate fuel mechanism with PAH and nitrogen oxide

* Corresponding author at Institute of Technology for Nanostructures (NST), Center for Nanointegration Duisburg-Essen (CENIDE), University of Duisburg-Essen, Duisburg, D-47057, Germany.
E-mail address: q.mao@itv.rwth-aachen.de (Q. Mao).

https://doi.org/10.1016/j.combustflame.2022.112574
0010-2180/© 2022 The Authors. Published by Elsevier Inc. on behalf of The Combustion Institute. This is an open access article under the CC BY license (http://creativecommons.org/licenses/by/4.0/)

Please cite this article as: R. Langer, Q. Mao and H. Pitsch, A detailed kinetic model for aromatics formation from small hydrocarbon and gasoline surrogate fuel combustion, Combustion and Flame, https://doi.org/10.1016/j.combustflame.2022.112574

chemistry and validated it against a comprehensive set of experimental data [37], including experimental data for various fuels and blends over a wide range of temperatures, pressures, dilutions, and equivalence ratios. A comparison of peak concentrations from experimental measurements and simulation results revealed a typical deviation of less than a factor of three for benzene, toluene, and styrene [37]. The average deviation factor for the two-ring species indene, naphthalene, and biphenyl increases to 5.5, significantly higher than the expected moderate increase due to the larger experimental uncertainty for species of higher molecular weight, thus, reflecting the incomplete understanding of the two-ring formation chemistry [36]. Furthermore, Dong et al. [37] show that the average deviation increases further with increasing molecular weight of PAH species, approaching an average deviation factor of 10 for a lumped $C_{12}H_8$ species [37], which the authors refer to as acenaphthalene. These results thus indicate a deterioration of the kinetic model performance for aromatic species with increasing molecular weight, in line with the assessment from Hansen et al. [36]. The considerable uncertainty in PAH species concentrations affects soot model predictions and necessitates further work on the chemical kinetic modeling of PAHs.

The high uncertainty in the acenaphthalene concentration is particularly troublesome due to the crucial role five-member rings play in theoretical [38–47] and recent experimental [48–50] works. The accurate prediction of acenaphthalene is, for example, highly relevant for the investigation of soot inception [38,46], as several proposed mechanisms involve partially embedded, peripheral five-member rings [38,46,51,52].

As Frenklach and Mebel [38] demonstrated, it was possible to critically review several proposed soot inception mechanisms without detailed chemical kinetic modeling of the gas phase. The criteria introduced by Frenklach and Mebel [38] narrow down potential soot inception mechanisms and suggest that a five-member ring present on a molecule's edge (e.g., acepyrene, A_4R_5) enables the most promising pathway [38]. Additionally, recent experimental studies by Commodo et al. [48] and Schulz et al. [49] provide evidence of aromatic and aliphatic five-member rings in the periphery of aromatic incipient soot molecules. Five-member rings also play an essential role in soot particle growth pathways, which can involve penta-ring migration on zigzag edges [40,42,43,45], transformations between five- and six-member rings [40,42,43], the flipping of five- and six-member rings [44], and pathways forming non-planar PAHs [46,53]. Due to several open questions related to the chemistry of partially embedded five-member rings, the model development will focus on acenaphthalene and other $C_{12}H_8$ isomer predictions.

Recently, Liu et al. [54,55] and Chu et al. [56] investigated Hydrogen-Abstraction-C_2H_2-Addition (HACA) routes for acenaphthalene formation. In addition, Savchenkova et al. [57] and Liu et al. [55] proposed reaction kinetics of subsequent acenaphthalene growth. As expected, due to the work of Frenklack et al. [40], their results highlight the importance of acenaphthalene formation through acetylene addition to 1-naphthyl radicals. However, the reaction kinetics [54,55,57] were merely tested in simulations of two premixed atmospheric pressure ethylene/oxygen/argon flames [17,58]. While these tests can be valuable for assessing the potential relevance of a new or updated pathway, validation against a larger dataset is required to determine impacts on chemical kinetic model development efforts due to the large uncertainty in the acenaphthalene prediction [37].

Several chemical kinetic models for surrogate fuel combustion were successfully validated against comprehensive experimental datasets, including PAH species mole fraction measurements [10,37,59,60]. These studies have introduced simplifications for the acenaphthalene chemistry to reduce computational effort, for example, by neglecting the potentially important pressure-dependence of reaction kinetics [59,60] or by lumping of $C_{12}H_8$ isomers [10,37]. It was demonstrated [10,37,59,60] that using these assumptions, species mole fractions of PAHs larger than acenaphthalene can still be predicted with sufficient accuracy for the considered application cases. Here, we want to focus on the chemistry of two- and three-ring species in a broad range of conditions and provide a more detailed description of their chemistry. The recently published model of Kukkadapu and co-workers [35,36] incorporates many reaction pathways and associated rate parameters from recent high-level quantum chemistry calculations into their model for surrogate components [61]. The comprehensive literature considered for their model [35,36] will also be relevant in the present work. Additionally, the present work emphasizes the formation and growth of acenaphthalene and its isomers by considering recently published theoretical studies [55,56].

The chemical kinetic model developed in the present work is based on the gasoline surrogate model published by Cai et al. [62], which builds on prior work, including the oxidation of small hydrocarbons [34], reactions of various substituted aromatic compounds [34,63], growth and oxidation chemistry of PAHs [34,63], and the oxidation of primary reference fuel (PRF) and PRF/toluene/ethanol mixtures [62,64]. The model of Cai et al. [62] and its predecessors were validated against comprehensive datasets that include experimental measurements for several different fuels relevant to the present work in a broad range of temperature and pressure conditions. Therefore, this model is a good starting point to develop an updated PAH chemistry model that incorporates the latest understanding of the chemistry based on recent ab-initio and experimental studies.

The study is composed of three sections. First, updates introduced in the model of Cai et al. [62] are explained. The second part presents a validation against ignition delay times, laminar burning velocities, and speciation data. Finally, the third part discusses reaction flux analyses for the formation of indene, naphthalene, and $C_{12}H_8$ isomers in counterflow flames.

2. Chemical mechanism

The present work intends to develop a chemical kinetic PAH model applicable to the broad range of pressures technically-relevant to combustion conditions. The origin of larger PAH species are reactions of species as small as acetylene or propargyl radicals [27,65], and PAH growth mechanisms, such as HACA [66], often require the availability of radicals. Consequently, PAH formation is highly sensitive to the main flame chemistry [14]. Therefore, and due to the hierarchical nature of combustion chemistry models [34], the first step of the model development was to update the reaction kinetics of elementary reactions in the core C_0–C_4 chemistry of the model published by Cai et al. [62].

The update process of some reactions was guided by the reaction kinetics selected for the NUIGMech1.1 chemical kinetic model [67–76], which was extensively validated against experimental measurements, including small and large hydrocarbons, in a broad range of conditions [67–70,72,73,76–82], and by the chemical kinetic model of Kukkadapu and co-workers [35,36]. Independent of both these models, reaction kinetics from the literature were incorporated. The importance of consistent thermodynamic and kinetic data is well known [8], and species thermochemistry was generally adopted from a study that proposed reactions kinetics. In case of missing thermochemistry for newly introduced species, the data is estimated through Benson group additivity with the implementation in the Reaction Mechanism Generator [83]. For several reactions, modifications introduced into the model of Cai et al. [62] were straightforward as merely a neglected pressure-dependence or more recent kinetic parameters were added. Such simple changes

are not discussed in the paper. Therefore, the original sources of the reactions and associated rate parameters are documented in the Chemkin input files for all updated reactions. In addition, the rate coefficients of about 10 reactions were adjusted within the uncertainties. The most significant adjustments are discussed in the paper, and all adjustments are reported in the Chemkin input files.

The Chemkin input files for the developed model, including the species thermochemical and transport data, are provided in the Supplementary Material. Additionally, the Supplementary Material includes a species dictionary with:

- Species names used in the chemical kinetic model
- International Chemical Identifiers (InChI) [84]
- Simplified molecular-input line-entry system (SMILES) formulas [85]
- Structural formulas [86]

The Supplementary Material also provides a python script that generates the species dictionary from the InChI- and SMILES-amended thermochemistry file. Species identifiers in ab-initio, experimental, and chemical kinetic model development studies are highly useful, and we hope the script might be helpful to others.

Abbreviated species names in the developed chemical kinetic model were generally introduced by prior work, either by Cai et al. [62] or the sources of reaction kinetics and thermochemistry. Most of the abbreviated names appearing in the discussion and the kinetic model follow the conventions introduced by Frenklach et al. [87] (e.g., A_1 for benzene, A_1- for phenyl, A_2 for naphthalene, A_2R_5 for acenaphthalene). Due to many sources for kinetic parameters, mixed naming conventions appear in the kinetic model.

The following discussion focuses on major modifications introduced into the model of Cai et al. [62] relevant to the prediction of PAH species.

2.1. Core C_0–C_4 chemistry

Allene, propyne. Allene (a-C_3H_4) and propyne (p-C_3H_4) are major intermediate species in the oxidation of heavier hydrocarbon fuels. H-abstraction from these molecules produces propargyl radicals (C_3H_3) [88], potentially leading to the formation of aromatic species. The model of Cai et al. [62] builds on the C_3H_4 chemistry developed by Blanquart et al. [34], which includes key reactions for the prediction of propargyl radicals, such as reactions on the C_3H_4 [89] and C_3H_5 [88] potential energy surfaces (PESs). However, the model of Cai et al. [62] does not consider results from more recent ab-initio studies that conducted high-level quantum chemistry calculations and provide temperature- and pressure-dependent rate coefficients for several important reactions, such as dissociation reactions of propargyl radicals [90], reactions on the C_3H_6 [91], C_3H_7 [92], and C_3H_8 [93] PESs, and reactions of propyne or allene with radicals other than hydrogen atoms [94–96].

The recently proposed chemical kinetic model for propyne oxidation and pyrolysis by Panigrahy et al. [72] considers the results from recent ab-initio studies [88–96]. Therefore, the developed chemical kinetic model adopted the C_3H_4 chemistry subset from the model of Panigrahy et al. [72]. Additionally, the recombination of allyl radicals [97], oxidation reactions of propene [98,99], and the oxidation of the C_3H_5 isomers [100,101] follow the model of Panigrahy et al. [72] as these subsets rely on reactions kinetics from recent ab-initio studies.

Diacetylene, vinylacetylene. Diacetylene (C_4H_2) and vinylacetylene (C_4H_4) concentrations are often similar to those of the C_3H_4 isomers. For example, peak mole fractions of diacetylene and vinylacetylene in counterflow flames of various fuels agree with allene and propyne within a factor of three [102–105]. Experimental [106] and theoretical [106–108] studies suggest that vinylacetylene-mediated growth reactions can contribute to the formation of naphthalene. Recent chemical kinetic modeling studies by Kukkadapu and co-workers [35,36,109] that were informed by theoretical results [110–113] revealed that the reaction $C_7H_5 \rightleftharpoons C_4H_2 + C_3H_3$ could produce fulvenallenyl radicals (C_7H_5), which can initiate naphthalene formation pathways [112]. The developed model considers this fulvenallenyl formation pathway with the reaction kinetics proposed by Derudi et al. [111]. Therefore, accurate chemical kinetic modeling of diacetylene and vinylacetylene is crucial to understanding the formation of PAH species.

The developed chemical kinetic model considers several possible formation pathways for vinylacetylene and diacetylene. The first pathway is the stepwise dehydrogenation of fuel or intermediate C_4 species such as 1-butene or 1,3-butadiene. H-abstraction reactions of stable species in these pathways are adopted from prior work, where the H-abstraction reactions from 1-butene are adopted from the model of Cai et al. [62], reactions with 1,3-butadiene are from the model of Zhou and co-workers [82,114], and the vinylacetylene subset is taken from Hansen et al. [36]. H-loss or addition reactions are included in the developed model as a part of reaction subsets derived from high-level quantum chemistry calculations on the C_4H_3 [115], C_4H_4 [116], and C_4H_5 [117] PESs.

Reactions of acetylene or ethylene with ethynyl radicals (C_2H) can be another source of diacetylene and vinylacetylene. In agreement with the experimentally observed hydrogen formation [118], the developed model considers the reaction $C_2H + C_2H_2 \rightleftharpoons C_4H_2 + H$ with the rate coefficient from Pedersen et al. [119]. Despite being about 27 kcal/mol exothermic from $C_2H + C_2H_2$ [118], Cai et al.'s model neglects the $C_4H_2 + H$ channel [34,62]. The C_4H_3 channels are considered in the developed model using the rate coefficients from the model of Panigrahy et al. [72].

A third reaction that can produce diacetylene is the decomposition of *ortho*-benzyne [120], where *ortho*-benzyne (O-C_6H_4) can be produced from the decomposition of benzyl radicals (A_1CH_2) [111] or the recombination of C_3H_2 (propynylidene) and C_3H_3 (propargyl radicals). The rate coefficients of reactions in the former pathway are based on high-level quantum chemistry calculations, and the latter recombination reaction is described by a rate coefficient estimate adopted from the chemical kinetic model of Hansen et al. [36].

The oxidation chemistry of diacetylene and vinylacetylene is adopted from the model of Hansen et al. [36], where most of the rate coefficients were taken by analogy to similar reactions, as only a few theoretical [121] and experimental results [122] are available in the literature. Oxidation of diacetylene by reactions with atomic oxygen [123] was neglected in the model of Hansen et al. [36], whereas it is considered in the developed chemical kinetic model. In the absence of experimental measurements or theoretical calculations for the several rate coefficients of significant reactions involving C_4 species and limited availability of validation targets for the developed chemical kinetic model, the overall uncertainty of this chemistry subset remains large.

1,3-Butadiene. Another important intermediate towards the formation of PAH is 1,3-butadiene (C_4H_6). H-abstraction from 1,3-butadiene produces C_4H_5 radicals [114,124,125], which enable benzene formation [126]. Additionally, dissociation reactions of 1,3-butadiene are important for the PAH growth chemistry as they can produce propargyl radicals [127]. As for the chemistry of C_3H_4 isomers, Cai et al. [62] adopted the 1,3-butadiene chemistry developed by Blanquart et al. [34]. More recently, Zhou et al. [82] developed a detailed chemical kinetic model for 1,3-butadiene chemistry. Sensitivity analyses revealed that reaction

kinetics from recent ab-initio and experimental studies are crucial for predictions of high-temperature chemistry [82], and the model of Cai et al. [62] is updated accordingly.

First, H-addition to the 1,3-butadiene double bonds, as investigated in theoretical calculations by Li et al. [125], enables significant 1,3-butadiene consumption pathways [82,125] and was included in the developed model. Furthermore, rate coefficients for H-abstraction of 1,3-butadiene by hydrogen [125] and hydroxyl [114] were updated. H-abstraction from the inner carbon atoms of 1,3-butadiene leads to the formation of the resonantly stabilized radical *i*-C_4H_5, which is mainly consumed by reactions with molecular oxygen [82]. The pressure- and temperature-dependent rate coefficients derived from the theoretical calculations of Rutz et al. [128] are used for the reactions in this subset. Additionally, low-temperature pathways initialized by the hydroperoxide addition to 1,3-butadiene were shown to have a significant impact on the fuel reactivity at around 1200 K and lower temperatures [82]. Despite the focus on high-temperature oxidation in the present work, this temperature range is relevant for the validation against measured ignition delay times, and the pathways were added to the developed model. The addition of atomic oxygen to 1,3-butadiene determines the reactivity at high temperatures, and reactions modeled by analogy to the corresponding propene reactions are adopted from Zhou et al. [82].

Thermal decomposition reactions of C_4H_6 isomers are taken from the model of Kukkadapu and co-workers [35,36]. The subset includes the reactions and the associated rate coefficients obtained from the experimental and theoretical work of Lockhart et al. [127].

Finally, the developed model includes pressure- and temperature-dependent rate coefficients calculated [56] from the C_4H_5 PES reported by Ribeiro and Mebel [117]. Reactions on the C_4H_5 PES, such as $C_2H_3 + C_2H_2 \rightleftharpoons n-C_4H_5$, are expected to be important for the prediction of laminar burning velocities of 1,3-butadiene [34] and resonance-stabilized radicals that can produce PAHs.

2.2. Oxidation of cyclic species

Cyclopentadiene. Cyclopentadiene (C_5H_6) and the resonance-stabilized cyclopentadienyl radical (C_5H_5) are considered important intermediates in the oxidation of benzene (A_1) as cyclopentadienyl is the product of unimolecular phenoxy radical (A_1O) decomposition [129–131]. Recent theoretical [132] and chemical kinetic modeling studies [36] highlight the importance of alternative phenoxy consumption pathways. They produce benzoquinone (OC_6H_4O) and cyclopentadienone (C_5H_4O), making cyclopentadienyl formation a minor channel. Still, understanding cyclopentadiene chemistry remains crucial, independent of its role during benzene oxidation, as five-member rings can be a part of a fuel component [133].

Reactions of cyclopentadienyl radicals have been proposed as part of PAH growth mechanisms such as the clustering of hydrocarbons by radical-chain reactions [134], naphthalene formation pathways [135], or ring-enlargement reactions [136]. These growth reactions [135,136] are included in the developed model and complemented by unimolecular reactions of cyclopentadienyl radicals [137] and reactions on the C_5H_7 PES investigated theoretically by Mao et al. [138]. Rate coefficients for H-abstraction reactions of cyclopentadiene based on theoretical calculations are taken from the work of Baroncelli et al. [133]. The reaction rate coefficient of $C_5H_5 + H$ association is based on that of Robinson and Lindstedt [139] but was increased by 25%. Reactions and associated rate coefficients for the oxidation of C_5H_5 are from recent theoretical studies by Mebel and co-workers [140–142], except for $C_5H_5 + HO_2$ reactions, which are taken by analogy to reactions of the allyl and hydroperoxide radicals (HO_2). Besides the H-addition reaction of cyclopentadiene, which is a part of the reactions investigated by Mao et al. [138] on the C_5H_7 PES, the addition of O and OH to cyclopentadiene and subsequent oxidation is incorporated into the developed model based on the NUIGMech1.1 model, which primarily builds on the work of Zhong and Bozzelli [130,131].

Cyclopentene. The cyclopentene (CYC_5H_8) subset was adopted from the model of Pejpichestakul et al. [10] with minor modifications. The validation in the present work is limited to two low-pressure counterflow diffusion flames investigated by Baroncelli et al. [133]. However, it is assumed that this validation is sufficient for the analysis of PAH growth, as Pejpichestakul et al. [10] previously investigated species mole fractions with the adopted subset in rich low-pressure premixed cyclopentene flames [143,144], where the relevant chemistry is similar.

Benzene. Benzene (A_1) is the smallest aromatic species, and several pathways involving benzene or the respective phenyl radical (A_1-) were proposed to explain PAH formation [66,108,145,146]. PAH growth is sensitive to flux through oxidation chemistry [36], and benzene oxidation reactions from the base model of Cai et al. [62] were updated in light of newer ab-initio calculations. Pratali Maffei et al. [147] computed rate coefficients for H-abstraction reactions of benzene at CCSD(T)/CBS//ωB97X-D/6-311+G(d,p) level of theory, which are adopted into the developed model.

One of the main reaction routes toward benzene oxidation is the addition of atomic oxygen to benzene [148], which is described with the reactions and rate coefficients computed by Cavallotti et al. [149], where the rate coefficient of the phenoxy-producing reaction $A_1 + O \rightleftharpoons A_1O + H$ was increased by 50% to decrease the deviation between measured and computed ignition delay times for lean mixtures. Reactions of phenol (A_1OH) and the calculated rate constants for the unimolecular decomposition of A_1OH and phenoxy radicals are adopted from the work of Pratali Maffei et al. [150]. The oxidation of phenyl and phenoxy radicals proceeds through the reactions on the $C_6H_5O_2$ PES investigated by Morozov et al. [132], where the rate coefficient of the reaction A_1- $+ O_2 \rightleftharpoons A_1O + O$ was increased by a factor of two.

At intermediate-to-low temperatures ($T < 1500$ K), here considered in the validation, the H-*ipso*-addition–elimination reaction ($A_1OH + H \rightleftharpoons A_1 + OH$) determines the reactivity of A_1OH. It is therefore included in the model, where the rate coefficient is from the work of Pratali Maffei et al. [151].

Toluene, fulvenallene. Toluene makes up 12% by weight of gasoline [63] and is a common component of gasoline surrogates [64]. Following recommendations from recent kinetic studies, the growth and oxidation reactions of toluene and the respective radicals were updated.

Rate coefficients computed from high-level quantum chemistry calculations [152,153] are adopted to describe the benzyl (A_1CH_2) or methyl-phenyl radical (A_1CH_3-) formation from H-abstraction reactions of toluene by OH, HO_2, O, O_2, CH_3, and H. The pressure- and temperature-dependent reaction kinetics describing the oxidation of benzyl radicals by O_2 are taken from Pelucchi et al. [152]. Methyl-phenyl radical oxidation by reactions with molecular oxygen is considered in the developed model with reactions and rate coefficients proposed by da Silva et al. [154]. Pathways initialized by reactions of $A_1CH_2 + HO_2$ [155] and the addition of atomic oxygen on the aromatic ring [156] are described as pressure-dependent in the developed model.

New rate coefficients derived from theoretical calculations were introduced for the reactions of the benzyl radicals with propargyl [157] and acetylene [145]. The H-*ipso*-substitution reaction on toluene ($A_1CH_3 + H \rightleftharpoons A_1 + CH_3$) is an important toluene consumption channel and is updated with rate coefficients computed by Pratali Maffei et al. [151]. Isomerization between methyl-phenyl and benzyl radicals is described with rate coefficients based on the theoretical calculation of Dames and Wang [158].

Recent chemical kinetic modeling studies revealed [35,36,109] that recombination reactions of fulvenallenyl (C_7H_5) and propargyl radicals (C_3H_3) are a potential naphthalene (A_2) formation pathway. An important source of fulvenallenyl radicals can be the dehydrogenation of benzyl radicals, a pathway that was neglected in the model of Cai et al. [62]. The reaction kinetics computed from an investigation of the C_7H_7 PES by Derudi et al. [111] describes the formation of fulvenallene (C_7H_6) in the first step. Reactions and rate coefficients determined by Cavallotti and co-workers [110,159] from theoretical calculations of the C_7H_6 PES and H-abstraction reactions of fulvenallene proposed by da Silva and Bozzelli [112] are used to model the formation of fulvenallenyl radicals. Oxidation reactions of fulvenallenyl are taken by analogy to cyclopentadienyl (C_5H_5).

Ethylbenzene. The homolysis reactions of ethylbenzene ($A_1C_2H_5$) have been replaced by the pressure-dependent description of this subset from the model of Yuan et al. [160]. Additionally, recombination reactions of benzyl and methyl investigated by Matsugi and Miyoshi [161] were added to the ethylbenzene chemistry.

Reactions on the C_8H_9 PES, such as reactions of A_1- + C_2H_4 and the decomposition of the phenylethyl radicals ($A_1CH_2CH_2$, A_1CHCH_3), are described with Chu et al.'s pressure-dependent rate coefficients [162]. Incorporating this reaction subset into the developed model and comparing flow reactor measurements [163] to simulation results in the temperature range 1060–1090 K, it was found that an accurate styrene ($A_1C_2H_3$) prediction requires a distinction between the two phenylethyl radicals. This observation is in line with the work of Chu et al. [162]. Analyzing their experiments conducted at a lower temperature range (600–800 K), Chu et al. [162] showed that the thermochemistry of both phenylethyl radicals sensitively affects styrene. Additionally, *ortho*-ethyl-phenyl ($A_1C_2H_5$-) reactions are introduced into the developed model, as *ortho*-ethyl-phenyl was experimentally observed [162] and affected styrene formation.

The thermochemistry of the newly introduced 1-phenylethyl (benzylic radical, A_1CHCH_3) and *ortho*-ethyl-phenyl radicals was adopted from Chu et al. [162]. Other C_8H_9 radicals considered by Chu et al. [162] were neglected in the developed model as they are expected to be insignificant. Required H-abstraction reactions of ethylbenzene producing 1-phenylethyl were adopted from the NUIGMech1.1 model [72]. Consumption reactions of the resonance-stabilized 1-phenylethyl are taken by analogy to reactions of the allyl radicals (A-C_3H_5). Reactions of *ortho*-ethyl-phenyl were taken by analogy to reactions of methyl-phenyl.

As for toluene, the *ipso*-substitution reaction $A_1C_2H_5$ + H $\rightleftharpoons$ A_1 + C_2H_5 can be a significant channel for benzene formation. The model uses the rate coefficient computed by Pratali Maffei et al. [151], increased by 50% to improve agreement with experimental flow reactor measurements.

Styrene. Recent work by Sikes et al. [164] showed the dissociation of styrene ($A_1C_2H_3$) to be a complex multichannel process with strong pressure and temperature dependencies. Following the assumption of Grela et al. [165], the dominant styrene decomposition channel in the model of Cai et al. [62] produces benzene and a vinylidene radical (H_2C_2) [62,63], independent of pressure. Other channels are considered, but they are insignificant. In contrast, Sikes et al.'s experimental and theoretical work [164] showed that the A_1 + H_2C_2 channel accounts for roughly 5% of styrene consumption, while the dominant pathways form styryl radicals. The developed model was updated according to the results of Sikes et al. [164].

The added subset includes unimolecular decomposition reactions of styrene and the isomerization and dissociation reactions of styryl radicals. The developed model considers channels for *ortho*-styryl ($A_1C_2H_3$-), resonance-stabilized 1-phenylvinyl (A_1CCH_2, α-styryl in Sikes et al. [164]), and 2-phenylvinyl (A_1CHCH, β-styryl in Sikes et al. [164]). Reactions of 1-phenylvinyl are considered due to their importance for styrene decomposition at the conditions investigated by Sikes et al. [164] (1800–2250 K and 60–240 Torr), while a detailed model for 2-phenylvinyl and *ortho*-styryl is required due to their importance for HACA routes [146]. Missing H-abstraction reactions of the styrene ring were taken by analogy to H-abstractions of the toluene ring. H-abstraction reactions producing 1-phenylvinyl are modeled using the rate coefficients for H-abstraction reactions of toluene producing benzyl, where rate coefficients were reduced by a factor of six to approximately account for the reduced number of available hydrogen sites, and the effects of the CH_2 group.

Sharma et al. [166] proposed the recombination of cyclopentadienyl and propargyl radicals as a styrene formation pathway. Reactions and rate coefficients derived from their investigation of the C_8H_8 PES were added to the developed model.

As theoretical or experimental studies on reactions of styrene with O and OH remain unavailable in the literature [63,167], reactions are mostly taken by analogy [63]. The addition of atomic oxygen to styrene is a key reaction in styrene oxidation, but theoretical investigations of this reaction class remain challenging [149,168]. Viable products are phenylethenols ($A_1C(OH)CH_2$, $A_1CHCHOH$) or vinylphenols, and the respective resonance-stabilized radicals in analogy to the main channels of O addition to benzene. Alternatively, benzyl and formyl or phenoxy and vinyl radicals might be produced through the cleavage of a C–C bond. The large uncertainty in the products sensitively affects the competition between chain termination and branching, and for simplicity, the current model introduces global reactions, where the total rate coefficient estimate of Lindstedt et al. [16] is adopted, but products were adjusted to match the experimental measurements.

Xylene. Minor changes were introduced to the xylene chemistry, such as an updated rate coefficient for the reaction $A_1(CH_3)_2$ + H $\rightleftharpoons$ A_1CH_3 + CH_3 [151].

Indene, naphthalene, and 1-methylnaphthalene. The kinetic data of one-ring species approximates that of two-ringed species [63] in the model of Cai et al. [62]. Therefore, the oxidation of indene (C_9H_8), naphthalene (A_2), and 1-methylnaphthalene (A_2CH_3) are updated according to the changes introduced to the cyclopentadiene, benzene, and toluene chemistry. The reaction of indenyl (C_9H_7) with molecular oxygen is described with the reaction kinetics proposed by Ghildina et al. [169]. Additionally, updates were introduced to the indenone chemistry. Indenone (C_9H_6O) is an essential intermediate in the oxidation of indene. Its consumption proceeds through unimolecular decomposition reactions modeled in analogy to reactions of cyclopentadienone (C_5H_4O) and reactions on the C_9H_7O PES described with the reaction kinetics computed by Ghildina et al. [170].

2.3. PAH chemistry

The present work emphasizes the development of a model for indene, naphthalene, and acenaphthalene formation. However, repetitive schemes of radical–radical and radical–molecule reactions [15,35,171] predict the growth of PAH species up to acepyrene (A_4R_5). The first step in this sequence is the formation of the first ring. The benzene and fulvene predictions rely on high-level quantum chemistry calculations following prior work [34,35]. The most important formation pathways are: C_3H_3 + C_3H_3 [172], acetylene + C_4H_5 [126], C_3H_3 + allyl radicals [173], and C_5H_5 + CH_3 [136]. The isomerization reactions between fulvene and benzene are from Miller et al. [172] and Jasper et al. [174].

Recent chemical kinetic modeling studies highlight the role of fulvenallenyl as an intermediate toward naphthalene for-

mation in pathways that potentially bypass benzene formation [35,36,109]. The discussion of the diacetylene [111,113] and toluene [110,112,159] chemistry in the previous Section 2.2 explains fulvenallenyl formation. Additionally, several minor molecular growth pathways, relying on estimated rate coefficients from the model of Kukkadapu et al. [35], describe the formation of other one-ringed species such as benzyne or benzyl.

Indene. Indene formation is updated based on recent advances. Reactions of the phenyl radicals initiate most of the newly added pathways. The developed model considers the following pathways: The association of A_1- + C_3H_3 with the reaction kinetics of Morozov et al. [175], growth reactions of phenyl with C_3H_4, C_3H_5, and C_3H_6 species with the reaction kinetics computed by Mebel et al. [145], the reaction $A_1C_2H + CH_3 \rightleftharpoons C_9H_8 + H$ [145], and association of $A_1 + C_3H_3$ [145]. The latter pathways were added for completeness, as Mebel et al. [145] expect insignificant indene formation from these reactions.

Indene formation from acetylene addition to resonance-stabilized C_7H_7 radicals, including benzyl, is described with the reaction kinetics computed in recent ab-initio studies [138,145]. Reactions of $C_5H_6 + C_5H_5$ were updated based on the recommendations of Cavallotti et al. [176]. Additionally, growth reactions of A_1- + C_4H_6, investigated by Fascella et al. [177], can produce indene and have been considered. Finally, the thermal decomposition kinetics of indenyl from the theoretical study of Sundar et al. [178] were incorporated. As the reactions proposed by Sundar et al. [178] are reversible, they potentially enable the formation of indenyl from the smaller species.

Naphthalene. Frenklach and co-workers [8,22,25,40,179,180] introduced the best-known molecular growth pathway for PAH species, HACA, a repetitive sequence of H-abstraction from a reacting hydrocarbon by a radical followed by the addition of acetylene to the radical site. Experimental [181] and theoretical [146,182] studies suggest various viable HACA routes from benzene to naphthalene exist. Chu et al.'s detailed pressure-dependent chemical kinetic model [56] builds on prior high-level quantum chemistry calculations [66,146,182] and adds new naphthalene reactions on the $C_{12}H_9$ PES. The developed model considers all HACA routes from the model of Chu et al. [56], which includes Frenklach's original route, the Bittner–Howard route, and the modified Frenklach route. In Frenklach's original route, the first acetylene addition produces phenylacetylene (A_1C_2H). Following H-abstraction of phenylacetylene, the second acetylene molecule adds to the ring, leading to the formation of naphthyl or naphthynes. In the Bittner–Howard route, the second acetylene molecule adds to the styryl radical 2-phenylvinyl (A_1CHCH), which produces naphthalene. The modified Frenklach route proceeds via *ortho*-styryl ($A_1C_2H_3$-). As for Frenklach's original route, the second acetylene molecule adds to the ring and produces naphthalene. Additionally, the developed model considers a pathway similar to Frenklach's original route [56], where second acetylene addition produces benzofulvenyl instead of naphthyl or naphthynes.

The addition of C_4 species to phenyl potentially leads to the formation of naphthalene. The role of vinylacetylene in naphthalene formation is investigated with the developed model using the reactions and rate constants from Mebel et al. [108]. Since vinylacetylene and diacetylene concentrations are in the same order of magnitude, the diacetylene addition to phenyl was investigated at M06-2X/6-311+G(d,p) level of theory [183] and included in the model. Additionally, the developed model considers reactions of phenylacetylene radicals and ethylene studied at CCSD(T)/CBS//ωB97X-D/6-311+G(d,p) level of theory [184].

The developed model includes reactions and rate coefficients from the theoretical investigation of Monluc et al. [107] that describe the direct formation of naphthyl radicals from reactions of ortho-benzyne and vinylacetylene.

Kukkadapu and co-workers [35,36,109] showed that ring-enlargement pathways initiated by the recombination of methyl and indenyl could significantly contribute to the formation of naphthalene. The modeled pathways [35] are based on recent experiments and computations by Zhao et al. [185] and included in the developed model.

Hansen et al. [36] highlighted the importance of benzyl and propargyl recombination reactions in their investigation of propyne-doped premixed toluene and benzene flames. The developed model adopts the respective reactions and rate coefficients, based in part on the work of Matsugi and Miyoshi [157], from the model of Hansen et al. [36].

Da Silva and Bozzelli [112] proposed the recombination reaction of fulvenallenyl and propargyl radicals as a possible molecular growth pathway. Following the chemical kinetic modeling study of Kukkadupa et al. [35], reactions and rate coefficients are taken by analogy to the recombination reactions of propargyl radicals [172].

Long et al. [135] investigated quantum chemical pathways for the recombination reactions of C_5H_5 radicals, which can initiate naphthalene formation pathways. They note that the previously adopted 1-step global reaction [34,62] leading to naphthalene and two H atoms may not be an adequate description [135]. Accordingly, the developed model includes the detailed pressure-dependent kinetics of Long et al. [135].

Following prior works [35,62], further growth of naphthalene and naphthyl radicals is modeled by analogy to benzene and phenyl reactions.

Biphenyl. The self-reaction kinetics of phenyl radicals producing biphenyl are taken from the combined experimental and theoretical work of Tranter et al. [186]. In addition, Kukkadapu et al. [35] showed that radical–radical recombination reactions of aliphatic C_9H_8 isomers [145,175] and propargyl, modeled by analogy to propargyl recombination, could be a significant biphenyl formation pathway, and the developed model includes this subset of reactions.

Acenaphthalene. Naphthalene growth via HACA routes can be a significant formation pathway for acenaphthalene [54,56]. The developed model considers these pathways [54,56] by including the detailed pressure-dependent kinetic model of Chu et al. [56] as a subset. Chu et al.'s model is based on high-level quantum chemistry calculations [54,56,187]. In addition to acenaphthalene formation, it describes the formation of $C_{14}H_8$ and $C_{14}H_{10}$ species in agreement with experimental measurements [50]. Recently, Liu et al. [55] investigated additional growth pathways of acenaphthalene, and the newly proposed pathways and rates complement the kinetics of Chu et al. [56]. Additionally, the developed model considers the formation of 1-phenanthrenyl radicals from 3-ethynylacenaphthalene via H-addition to the five-membered ring, followed by a ring flip, as proposed by Savchenkova et al. [57].

In an investigation of phenalene (A_2C_6) formation, Zhao et al. [188] explored growth reactions of 1-naphthyl radicals with propyne and allene. The developed model includes the proposed reactions and rate coefficients derived from their theoretical calculations, where some of the reactions produce 1-methylacenaphthalene (MEA_2R_5) and acenaphthene. In addition, 2-naphthyl radical growth reactions [189] are modeled by analogy to the similarly fast 1-naphthyl growth reactions [188], where 2-ethynylnaphthalene (A_2C_2HB) replaces acenaphthalene as a product.

Based on a theoretical investigation, Porfiriev et al. [190] propose that the recombination reaction of 1-acenaphthyl (N1-CS41) and methyl radicals can enable phenalenyl radical formation pathways. The developed model includes the reaction kinetics computed by Porfiriev et al. [190]. However, a revision might be necessary due to considerable uncertainty in some of the rate

coefficients, as Porfiriev et al. [190] discussed. Mass spectra observed by Levey et al. [191] combined with theoretical calculations suggest that the CH cycloaddition mechanism is a viable pathway from five-membered to six-membered rings. However, the kinetics of the proposed pathway are unavailable and therefore not yet considered.

Repetitive schemes based on growth reactions of smaller species model additional growth pathways of acenaphthalene following Cai et al. [62] and Hansen et al. [36].

Phenanthrene. Kukkudapu et al. [35] proposed reactions of phenyl with phenylacetylene as a potentially significant phenanthrene formation pathway. In the developed model, reactions and rate coefficients for this pathway are taken from the theoretical investigation of Tuli and Mebel [192]. Yang et al.'s rates [193] describe HACA pathways producing phenanthrene from biphenyl.

Following Kukkadapu et al. [35], the recombination of fulvenallenyl radicals can produce phenanthrene in analogy to propargyl recombination reactions. The chemical kinetic modeling of allene and propyne flames [35] suggests that benzo-indenes, such as fluorene, constitute a significant portion of the experimentally measured mole fraction of $C_{13}H_{10}$ isomers. As ring-enlargement pathways of indene can significantly contribute to naphthalene formation [35,36,109], by analogy, benzo-indene formation and growth through ring-enlargement are expected to contribute to the phenanthrene formation. As recent chemical kinetic modeling studies confirm the significance of benzo-indene formation and growth pathways [35,109], the developed model includes this subset from the model of Hansen et al. [36].

Large PAH species. The developed model uses consistent rate coefficients for the formation pathways of large stabilomers [194,195] (aceanthrylene, acephenanthrylene, pyrene, acepyrene) and fluoranthene taken by analogy to reactions of similar smaller species.

The oxidation of PAHs follows the models of Cai et al. [62] and Hansen et al. [36].

The final model consists of 1036 species connected via 6139 reactions. The developed model's reaction and rate coefficients are all below the collision limit [196] between 700 and 2500 K in the pressure range 0.039–100 atm. A detailed report on the collision limit violations in the temperature range 500–3000 K is provided in the Supplementary Material, where violations do not exceed a factor of 10 and occur for 33 reactions. Therefore, the collision limit violations are not expected to affect the results.

3. Validation results

The updates introduced to the model of Cai et al. [62] affect the oxidation and growth chemistry of several species. Accordingly, a comprehensive validation covering all relevant fuels in a broad range of temperatures and pressures is required. At the same time, it is necessary to consider that the model developed in the present work builds on a detailed chemical kinetic model [62], which was extensively validated in prior works [34,62–64]. Table 1 lists the validation cases considered in the present study. The model of Cai et al. [62] was previously validated against several of the validation tests in Table 1 [34,62–64], and, except for the cyclopentene cases, it is applicable in the entire range of experimental conditions. Therefore, prediction errors of the model of Cai et al. [62], given by deviations between computed and measured results, can be utilized to enhance and simplify the validation of the updated model. On the one hand, the prediction errors of the model of Cai et al. [62] serve as a benchmark for the developed model. On the other hand, if differences in the prediction errors of both models are insignificant for previously considered validation cases, a discussion is omitted to avoid redundancy.

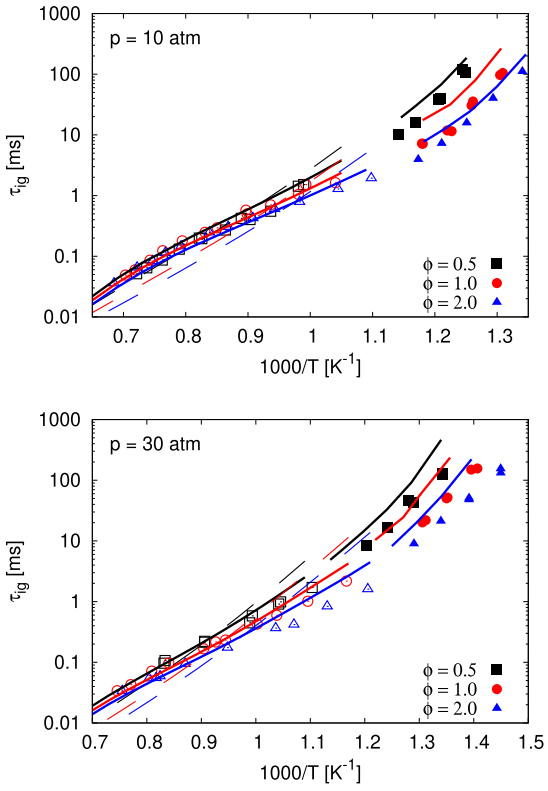

Fig. 1. Ignition delay times of propyne/air mixtures for three fuel-air-equivalence ratios (ϕ). Symbols denote experimental measurements by Panigrahy et al. [72] obtained using a rapid compression machine (filled) or a high-pressure shock tube (open). Solid lines show predictions of the model developed in the present work and dashed lines show the predictions of the model of Cai et al. [62].

The Supplementary Material provides a detailed graphical comparison of the experimental measurements, predictions from the model of Cai et al. [62], and predictions from the developed model for all cases listed in Table 1. Cai et al.'s model [62] and the developed model predict similar ignition delay times and laminar burning velocities for C_1–C_2 fuels, propane, propene, cyclopentadiene, benzene, 1-methylnaphthalene, *n*-heptane, iso-octane, and toluene. Furthermore, differences in the prediction errors are insignificant for species mole fractions for the oxidation of gasoline surrogate fuel mixtures in plug flow and jet-stirred reactors. The vast majority of these validation cases have been considered previously, and the reader is referred to prior works for a discussion [34,62–64].

The remaining validation proceeds in the same order as the model development section. The first part considers oxidation chemistry validation targets, including ignition delay times, laminar burning velocities, and speciation data from reactors for fuels of increasing molecular weight. The second part evaluates speciation data from 31 counterflow flames in a broad range of conditions as validation targets for the developed PAH chemistry.

3.1. Core C_0–C_4 chemistry

Significant differences between the models occur in the predictions of propyne oxidation validation targets. Figure 1 compares measured [72] ignition delay times to predictions of the developed model and the model of Cai et al. [62]. The model of Cai et al. [62] underpredicts measured ignition delay times for initial temperatures above 1100 K. Ignition delay times are overpredicted at lower temperatures, or no ignition occurs. The deviation between experimental measurements and the predictions

Table 1
Experimental conditions for the model validation sorted by fuel composition and pressure. The Supplementary Material describes the details of the simulations. + indicates a blend, and / signifies an alternative fuel composition. The type column introduces a distinction between ignition delay times (IDT), laminar burning velocities (SL), and speciation data from flow reactors (FR), counterflow flames (CF), or jet stirred reactors (JSR). p is the pressure.

Fuel composition	Type	p [bar]	References for experimental measurements
n-heptane	IDT	3, 13.5, 42	Ciezki and Adomeit [201], Minetti et al. [202]
	SL	1–25	Ji et al. [203], Jerzembeck et al. [204]
	CF	1	Wullenkord et at. [102]
iso-octane	IDT	13, 40	Fieweger et al. [205]
	SL	10–25	Jerzembeck et al. [204]
n-heptane + iso-octane+toluene	IDT	10, 30, 50	Fikri et al. [206]
	SL	1	Dirrenberger et al. [207]
	FR	12.7	Chaos et al. [208]
n-heptane + iso-octane + toluene + ethanol	IDT	10, 30, 50	Cancino et al. [209]
	SL	1	Dirrenberger et al. [207]
n-heptane + iso-octane	IDT	40	Fieweger et al. [205]
	JSR	1, 10.1	Chen et al. [210], Dagaut et al. [211]
	SL	1–25	Bradley et al. [212], Jerzembeck et al. [204]
ethylene + toluene	CF	1	Carbone and Gomez [103]
methanol	IDT	1.2, 2	Bowman [213], Noorani et al. [214]
ethanol	IDT	1, 2	Natarajan and Bhaskaran [215]
	SL	1, 10	Veloo et al. [216], Beeckmann et al. [217]
methane	IDT	2	Seery and Bowman [218]
	SL	1	Vagelopoulos and Egolfopoulos [219], Hassan et al. [220], Rozenchan et al. [221], Bosschaart and de Goey [222]
acetylene	IDT	1, 1.2, 2	Hidaka et al. [223], Rickard et al. [224]
	SL	1	Egolfopoulos et al. [225], Jomaas et al. [226]
acetylene (+ methane in one flame)	CF	1	Baroncelli et al. [227]
ethylene	IDT	1.2, 2	Horning et al. [228], Hidaka et al. [229]
	CF	1–25	Figura and Gomez [105], Carbone et al. [230]
	SL	1, 5	Egolfopoulos et al. [225], Jomaas et al. [226], Hirasawa et al. [231], Kumar et al. [232]
ethane	IDT	1.11	Vries et al. [233]
	SL	1, 5	Vagelopoulos and Egolfopoulos [219], Hassan et al. [220], Bosschaart and de Goey [222], Jomaas et al. [226]
propyne / allene	IDT	2.1–30.4	Curran et al. [234], Panigrahy et al. [72]
	CF	0.93	Kukkadapu et al. [35]
	SL	1, 2	Davis et al. [197], Panigrahy et al. [72]
propene	IDT	1, 4	Qin et al. [235]
	SL	1, 5	Jomaas et al. [226], Davis et al. [197], Saeed and Stone [236]
propane	IDT	2.5, 7, 8	Brown and Thomas [237], Burcat et al. [238]
	SL	1, 5	Vagelopoulos and Egolfopoulos [219], Bosschaart and de Goey [222], Jomaas et al. [226], Vagelopoulos et al. [239]
1,3-butadiene	IDT	2–41	Zhou et al. [82], Li et al. [240]
	SL	1, 5	Davis and Law [241], Zhou et al. [82]
	CF	1	Moshammer et al. [242]
1-butene / 1-butene + acetylene / 1-butene + methane / 1-butene + propene	CF	1	Baroncelli et al. [243]
cyclopentadiene	IDT	1	Orme et al. [244]
	SL	1	Ji et al. [245]
	FR	1	Butler et al. [198]
	JSR	1	Wang et al. [199]
cyclopentene	CF	0.08	Baroncelli et al. [133]
benzene	IDT	2.3–9	Burcat et al. [246], da Costa et al. [247]
	JSR	0.48, 1	Chai et al. [248], Ristori et al. [249]
	FR	1	Brezinsky [250]
	SL	1, 3	Davis and Law [241], Johnston and Farrell [251]
toluene	IDT	1.9–52	Burcat et al. [246], Shen et al. [252], Vasudevan et al. [253] (IDT and OH mole fraction profiles), Zhang et al. [254]
	FR	1	Klotz et al. [255]
	SL	1, 3	Hirasawa et al. [231], Davis and Law [241], Johnston and Farrell [251]
1-methylnapthalene	IDT	13	Pfahl et al. [256]
	JSR	1, 10.1	Mati et al. [257]
ethylbenzene	IDT	12, 40	Shen and Oeslschlaeger [258]
	FR	1	Litzinger et al. [163]
	SL	1, 3	Johnston and Farrell [251], Meng et al. [259], Mehl et al. [260]
m-xylene / *o*-xylene / *p*-xylene	IDT	1–10	Battin-Leclerc et al. [261], Gail et al. [262], Gail et al. [263], Shen and Oehlschlaeger [252]
m-xylene	FR	1	Emdee et al. [264]
m-xylene	SL	1, 3	Johnston and Farrell [251], Ji et al. [265]
styrene	IDT	1.43	Comandini et al. [266]
	FR	1, 40	Litzinger et al. [163]
	SL	1, 3	Comandini et al. [266], Meng et al. [259]

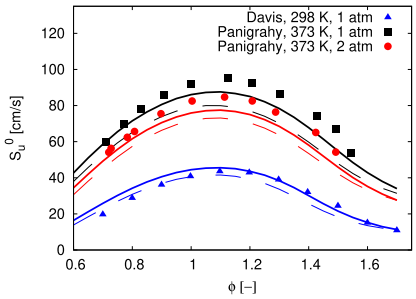

Fig. 2. Laminar burning velocities of propyne/oxygen/nitrogen mixtures. Experimental data from Panigrahy et al. [72] are for propyne/air mixtures. Davis et al. [197] used an oxidizer with an O_2 mole fraction of 18%. Solid lines show predictions of the model developed in the present work and dashed lines show the predictions of the model of Cai et al. [62].

of the updated model decreased significantly for all considered conditions, which results from ignition delay times being sensitive to the updated reaction kinetics of $p-C_3H_4$+HO_2 [72] and $p-C_3H_4$+OH [94].

The comparison of measured and computed laminar burning velocities of propyne/oxygen/nitrogen mixtures in Fig. 2 shows that prediction errors of the updated model decreased for most of the considered conditions. The laminar burning velocity is sensitive to the recombination reaction of propargyl and hydrogen radicals [172] and the reaction $p-C_3H_4+H \rightleftharpoons CH_3+C_2H_2$ [88]. The developed model adopts the rate coefficient adjustments introduced by Panigrahy et al. [72] to the reaction kinetics from Refs. [88,172]. In addition to decreased prediction errors in laminar burning velocities, the adjustments also decreased the deviation between computed and measurement benzene mole fractions for the considered 31 counterflow flames.

The present work introduced several updates to the 1,3-butadiene oxidation chemistry. While the differences between both models are minor for predictions of laminar burning velocities, prediction errors of the updated model decreased for high-pressure ignition delay times as shown in Fig. 3. The predictions are closer to experimental measurements in the considered temperature range due to the added pathways initialized by hydroperoxide addition to 1,3-butadiene [82]. Differences between model predictions can also be observed for species mole fractions in counterflow flames. Discrepancies between computed and measured species mole fractions are significant in both cases, as shown in Figs. S59 and S60.

3.2. Oxidation of cyclic species

Several updates were introduced to the oxidation chemistry of cyclic species. As evident from the detailed comparison in the Supplementary Material, both models' prediction errors are of similar magnitude for most cyclopentadiene, benzene, and toluene tests. The discussion focuses on two examples that highlight the updates' effects, which are cyclopentadiene and benzene oxidation in a flow reactor.

Figure 4 shows experimental measurements from the Princeton adiabatic, atmospheric pressure flow reactor [198] and model predictions for the C_5H_6 oxidation. The changed predictions, which are, in this case, closer to the experimental measurements, illustrate the effects of several updates. The fuel consumption is determined by the revised cyclopentadiene oxidation chemistry, which considers recent ab-initio studies [133,137,138,140–142]. Species mole fractions of substituted aromatic species, such as toluene (A_1CH_3), styrene ($A_1C_2H_3$), and phenylacetylene (A_1C_2H), are sensitively affected by newly introduced isomerization [164] or growth reactions [166] and the revised indene oxidation chemistry, which follows recommendations based on quantum chemistry calculations [169,170]. Guided by theoretical results [136], methylcyclopentadiene ($C_5H_5CH_3$) was added to the developed model to describe benzene formation and can now be validated against experimental measurement, as shown in Fig. 4. Despite the many advances, there is still considerable uncertainty in the simulation results, which explains underpredicted intermediate species in jet-stirred reactor simulations compared to experimental measurements [199], as shown in Figs. S72–S74.

Predictions of speciation data for benzene oxidation at atmospheric pressure improved with the updated model, as exemplified by the comparison of plug flow reactor measurements [200] and computed results shown in Fig. 5. All significant oxidation pathways of benzene are modeled with reactions and rate coefficients derived from high-level quantum chemistry calculations [132,147,149–151]. The improved predictions reflect the reduced uncertainty in rate coefficients and product branching fractions of the addition reaction of A_1 + O [149].

In some cases, the predictions of ignition delay times, laminar burning velocities, and speciation data from flow reactors of mixtures containing 1-methylnaphthalene, ethylbenzene, xylene, or styrene changed. However, no general trends for the agreement between model predictions and experimental measurements are evident from Figs. S96 to S115. Overall, the prediction accuracy of the developed model is similar to the model of Cai et al. [62] for 1-methylnaphthalene, ethylbenzene, xylene, and styrene oxidation. Key reactions for predicting the considered validation targets are reactions of these fuels with O and OH radicals. These reactions remain estimated by analogy to reactions of smaller fuels, implying significant uncertainty in the rate coefficients and assumed products. As the differences between the predictions of both models [62] are minor compared to the effects of uncertainties in estimates, we refrain from a detailed discussion.

Overall, prediction errors of the updated model and the model of Cai et al. [62] are of similar magnitude for the considered oxidation validation targets.

3.3. PAH chemistry

Several studies [35,133,227,243] showed that a PAH model's parameters and assumptions sensitively affect mole fraction predictions of aromatic species in counterflow flames. Dong et al. [37] compared peak mole fractions from a comprehensive set of experimental data to simulation results obtained with a newly developed detailed chemical kinetic model. It was demonstrated that parity diagrams showing the respective peak values allow for a compact visualization of a model's prediction accuracy and identification of systematic deviations. Therefore, measured peak species mole fractions of selected PAH species from 31 counterflow flames serve as validation targets for the developed PAH chemistry. Table 1 lists the considered fuel components and pressures. The following discussion focuses on the prediction of peak mole fractions. A detailed graphical comparison of computed and measured results and information on the simulations are provided in the Supplementary Material for all considered flames. The comparison also includes a few measurements of aromatic species from flow and jet-stirred reactors, which will not be discussed.

Additionally, the validation approach is extended to account for the estimated experimental uncertainty and the number of measurements available for a set of parameters defining a validation test case. Although not commonly acknowledged by chemical kinetic modeling studies, it is clear that the validation of a developed model aims to measure the error between a deterministic computational result and the mean of a population of experimental mea-

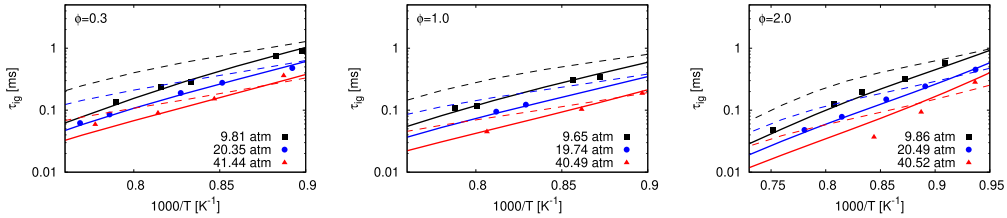

Fig. 3. Ignition delay times of 1,3-butadiene/air mixtures. Symbols denote high-pressure shock tube measurements from Zhou et al. [82]. Solid lines show predictions of the model developed in the present work and dashed lines show the predictions of the model of Cai et al. [62].

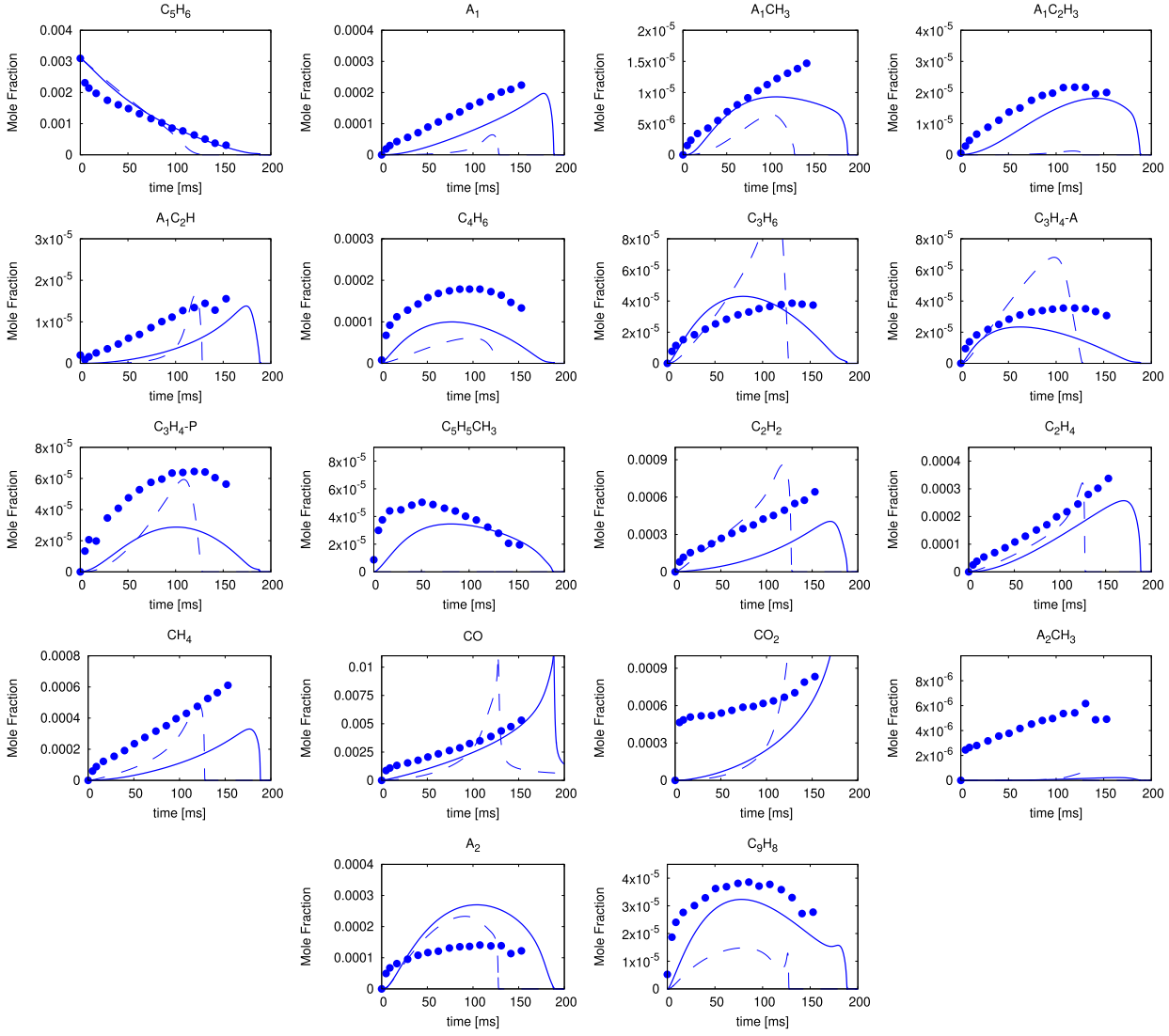

Fig. 4. Comparison of speciation data measured by Butler et al. [198] in the Princeton plug flow reactor (symbols), predictions of the model developed in the present work (solid lines), and the predictions of the model of Cai et al. [62] (dashed lines) for the oxidation of stoichiometric cyclopentadiene/oxygen/nitrogen mixture at 1 atm. Initial mole fractions and temperature: cyclopentadiene 0.3097%, O_2 1.9931%, N_2 97.697%, 1151 K. The experiments are modeled as an isobaric and adiabatic reactor.

surements for which only a finite sequence of measurements was obtained. As explained by Oberkampf and Barone [267], the key issue is the statistical nature of the sample mean of the measured quantity, not the accuracy of the agreement between the computational result and the individual measurements. Unfortunately, the sample size of the experimentally measured species mole fractions is usually small, as experimental studies rarely focus on reproducing measurements at previously considered boundary conditions. However, many experimental studies test the repeatability and report uncertainty estimates [35,230,243], which are the bases of quantitative error estimation.

The present work accounts for the statistical nature of the experimental measurements. It defines the estimated error as

$$\tilde{E}(x) = X_s(x) - \bar{X}_e(x), \tag{1}$$

where X_s is a peak species mole fraction from the simulation and $\bar{X}_e$ is the sample mean of the peak mole fraction based on n experiments conducted. The species mole fractions are functions of

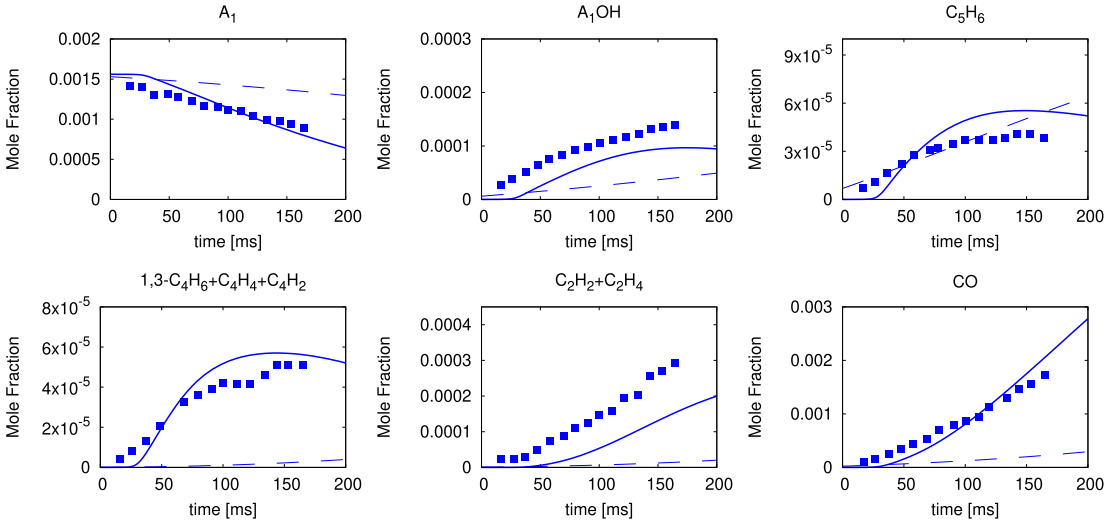

Fig. 5. Comparison of speciation data measured by Lovell et al. [200] in the Princeton plug flow reactor (symbols), predictions of the model developed in the present work (solid lines), and the predictions of the model of Cai et al. [62] (dashed lines) for the oxidation of stoichiometric benzene/oxygen/nitrogen mixture at 1 atm. Initial mole fractions and temperature: benzene 0.156%, O_2 1.17%, N_2 98.674%, 1102 K. The experiments are modeled as an isobaric and adiabatic reactor and the predicted species mole fractions were shifted by −40 ms.

parameters x defining a test case, reported in the experimental work and adopted as input to the simulations. The dependence on x is omitted in the following for clarity. The population's true mean from the experimental measurements μ_e remains uncertain for a finite number of measurements. However, a confidence interval (CI) can be estimated as [267, 268]

$$\mu_e \sim (\bar{X}_e - E_m, \bar{X}_e + E_m), \tag{2}$$

for a chosen level of confidence $C = 100(1-\alpha)$ %, where

$$E_m = t_{\alpha/2,\nu} \cdot \frac{s}{\sqrt{n}} \tag{3}$$

is the error bound of the mean, $t_{\alpha/2,\nu}$ is the $1-\alpha/2$ quantile of the t distribution [268] for $\nu = n-1$ degrees of freedom, and the sample standard deviation from the measured samples $X_e^1, X_e^2, \ldots, X_e^n$ is

$$s(x) = \left(\frac{1}{n-1} \sum_{i=1}^{n} \left(X_e^i - \bar{X}_e \right)^2 \right)^{1/2}. \tag{4}$$

The confidence interval for the true error is [267]

$$E = X_s - \mu_e \sim \left(\tilde{E} - E_m, \tilde{E} + E_m \right). \tag{5}$$

As species mole fractions of PAHs span more than three orders of magnitude for the considered conditions, focusing on the species mole fractions ratios is helpful rather than using the absolute error estimate in Eq. (1). If the simulations underpredict the mean of the sampled species mole fractions, the considered estimated error metric is the ratio $\bar{X}_e/X_s$ with the confidence interval of its true value given by

$$\frac{\mu_e}{X_s} \sim \left(\frac{\bar{X}_e - E_m}{X_s}, \frac{\bar{X}_e + E_m}{X_s} \right). \tag{6}$$

The inverse ratio $X_s/\bar{X}_e$ is used for overprediction with the respective confidence interval

$$\frac{X_s}{\mu_e} \sim \left(\frac{X_s}{\bar{X}_e + E_m}, \frac{X_s}{\bar{X}_e - E_m} \right). \tag{7}$$

The distinction between over- and underprediction avoids a one-sidedly bounded penalization associated with using the same denominator in both cases. The estimated mean deviation factor, defined as

$$\bar{R}_i = \frac{1}{m} \sum_{j=1}^{m} \max \left(\frac{\bar{X}_{e,i}(x_j)}{X_{s,i}(x_j)}, \frac{X_{s,i}(x_j)}{\bar{X}_{e,i}(x_j)} \right) \tag{8}$$

for parameters $x_1, x_2, \ldots, x_m$ defining the respective test cases, constitutes a one-number summary of the estimated error in the predictions of a species i. Confidence indicators for the true mean deviation factor are estimated by averaging widths between $\bar{X}_{e,i}(x_j)/X_{s,i}(x_j)$ and the bounds from Eq. (6) or $X_{s,i}(x_j)/\bar{X}_{e,i}(x_j)$ and Eq. (7).

Eqs. (3) and (5)–(7) show that estimating a confidence interval for the true error of model predictions is inherently based on the nature of the population of experimental measurements and requires a sample of known size and standard deviation. Most of the considered experimental studies estimate that the uncertainty in the measurements lies within a factor of two [35,230,243]. For simplicity, it is assumed that the underlying sample for those estimates has a size of $n = 2$. Assuming further, the uncertainty factor of two applies to every measurement i conducted, that is, $X_e^i/\bar{X}_e = 2$, the error bound in Eq. (3) simplifies to $E_m = t_{\alpha/2,1}\bar{X}_e = 0.3175\bar{X}_e$ for a $C = 90\%$ confidence level.

Several studies provide significantly smaller uncertainty estimates than what is assumed in the present work. However, it remains often unclear how these estimates were obtained. Sometimes, estimates are determined rigorously, but merely a subset of the potential sources of uncertainties affecting a measurement is considered.

Figure 6 compares measured and computed peak species mole fractions for the 31 counterflow flames listed in Table 1. The considered species are cyclopentadiene (C_5H_6), benzene (C_6H_6), toluene (A_1CH_3), phenylacetylene (A_1C_2H), styrene ($A_1C_2H_3$), ethylbenzene ($A_1C_2H_5$), indene (C_9H_8), naphthalene ($C_{10}H_8$), and acenaphthalene ($C_{12}H_8$), where either the listed species or isomer mole fractions are shown depending on the experimental measurement. Additionally, Fig. 6 shows the mean prediction error computed for the present model and the model of Cai et al. [62]. The prediction error decreased for all considered species mole fractions except for a slightly increased error for toluene (A_1CH_3).

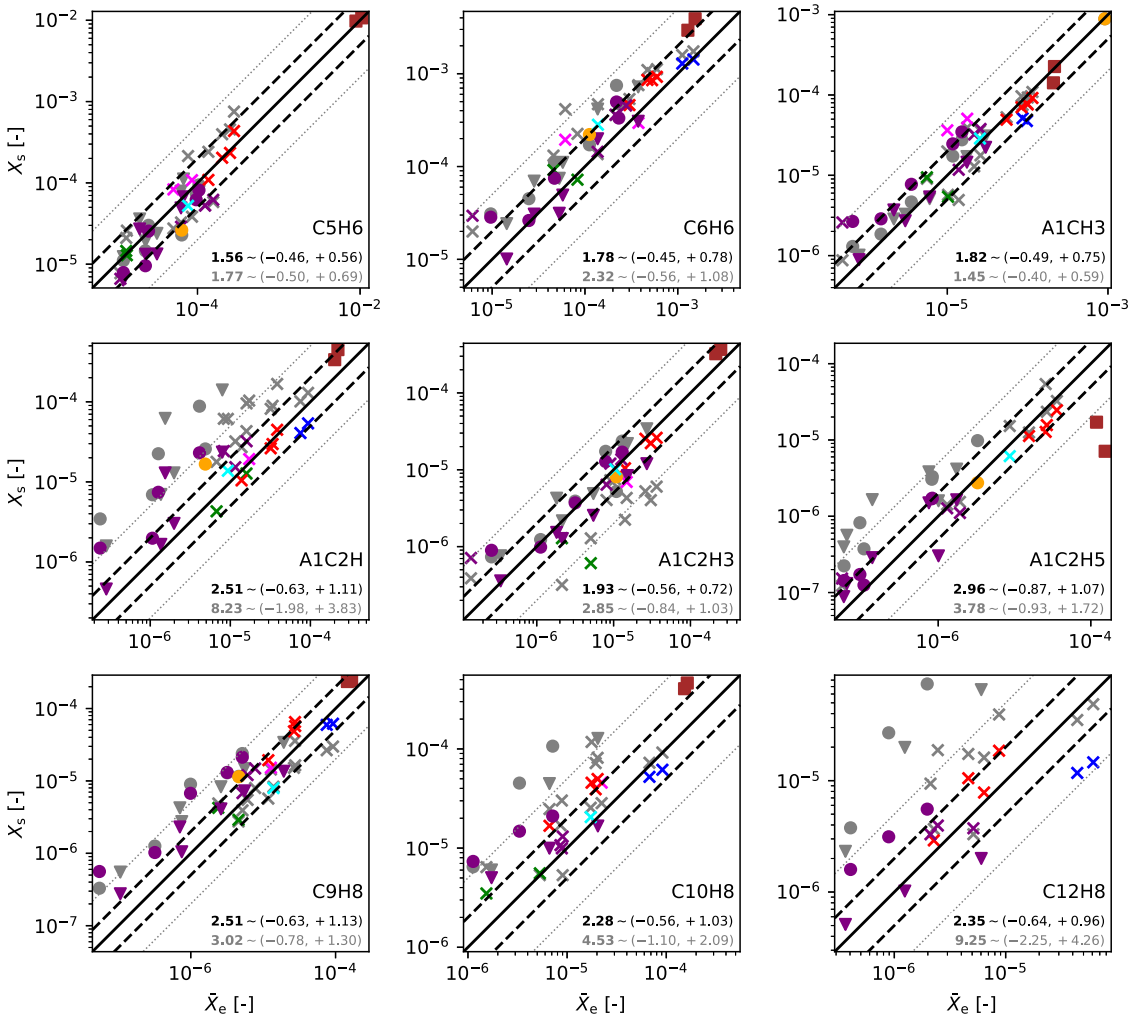

Fig. 6. Parity diagrams comparing peak mole fractions from experimental measurements to simulation results, where single species or isomer mole fractions were selected as appropriate for the respective experiment. Dashed lines indicate a deviation of a factor of two, and dotted gray lines a factor of five. Results obtained with the chemical kinetic model from the present work use colors representing the fuel composition, magenta: 1,3−butadiene [242], green: acetylene [227], blue: allene or propyne [35], red: 1−butene or 1−butene blends [243], purple: ethylene [105,230], orange: toluene – doped ethylene [103], brown: methane – doped cyclopentene[133], cyan: *n*−heptane [102]. Results obtained with the model of Cai et al. [62] are shown in gray. The symbol shape represents the pressure, ■ 80 mbar, $\times p \approx 1$ bar, • 2 bar $\leq p \leq$ 4.1 bar, ▼$p \geq$ 8 bar. Values in the bottom right are: $\bar{R}_i$ from Eq. (8), the average width between the CI bound closer to 1 and $\bar{R}_i$, and the average width between $\bar{R}_i$ and the CI bound further apart from 1 (confidence level $C = 90\%$, individual CI bounds from Eqs. (6), (7)). The upper row in black is computed with the predictions of the model from the present work, and the lower row in gray is computed with predictions from the model of Cai et al. [62]. (For interpretation of the references to color in this figure legend, the reader is referred to the web version of this article.)

The deterioration of the mean toluene prediction error can largely be attributed to the overprediction of peak mole fractions in the 1,3-butadiene diffusion flames and some of the ethylene flames. The update process of the model showed that the changes in the C_4-part of the mechanism affect predictions of toluene and other aromatic species. Important oxidation reactions in the high-temperature chemistry of 1,3-butadiene, such as the addition of oxygen atoms to 1,3-butadiene, the oxidation chemistry of vinylacetylene, and most of the oxidation chemistry of diacetylene are estimated by analogy to presumably similar reactions reflecting the current literature knowledge [36,82,114]. The same subset of reactions becomes relevant in ethylene flames as the reactions $C_4H_6 + H \rightleftharpoons C_2H_4 + C_2H_3$ and $C_2H_4 + C_2H \rightleftharpoons C_4H_4 + H$ produce C_4 species. The former reaction was missing in the model of Cai et al. [62]. It increased the predicted 1,3-butadiene mole fraction by more than an order of magnitude in some of the considered ethylene flames, improving the agreement with experimental measurement in most cases considerably, as shown in the Supplementary Material. Hence, remaining uncertainties in the high-temperature oxidation of C_4 species can affect the predictions of aromatic species and should be addressed in future work.

The C_5H_6, C_6H_6, A_1CH_3, and $A_1C_2H_3$ peak mole fractions deviate on average less than a factor two from the measurements. The average deviation factor increases to 2.5 for indene, naphthalene, and acenaphthalene. Previous studies demonstrated that the prediction of acenaphthalene can be challenging [37,230]. Albeit for a smaller dataset than for the other species' mole fractions, the comparison in Fig. 6 indicates that the model updates introduced in the present work improve the predictions substantially.

Surprisingly, the most significant error is observed for the smaller substituted aromatic species ethylbenzene instead of the two- and three-ring species. However, most predicted ethylbenzene mole fractions agree with the measurements within a factor of two. The relatively large average deviation is caused by a severe underprediction of ethylbenzene in low-pressure cyclopentene flames. The significant discrepancy might be due to the relatively simple cyclopentene subset and its limited validation. Miss-

ing ethylbenzene formation pathways enabled by five-member ring species are another possible explanation. The dominant styrene formation pathways in the cyclopentene flames are initiated by the recombination of cyclopentadienyl and propargyl radicals [166]. Analogous growth pathways are not considered for ethylbenzene.

On average, peak mole fractions of phenylacetylene are 2.51 times higher than the experimental measurements, which is significantly lower than the prediction error of the model of Cai et al. [62] but somewhat larger than the developed model's prediction error for toluene and styrene mole fractions. The dominant phenylacetylene formation pathway is acetylene addition to phenyl radicals. The relevant reactions are described with rate coefficients based on high-level quantum chemistry calculations [146,147]. However, the rate coefficient of the most significant phenylacetylene oxidation reaction, $A_1C_2H + OH \rightleftharpoons A_1 + HCCO$, was estimated [269] and increased in the present work by a factor of five to decrease the deviation between measured and computed peak mole fractions. Without the adjustment, the average deviation would increase to a factor of 3.75 for the updated model, still significantly lower than the average deviation of 8.23 for the model of Cai et al. [62]. However, the uncertainty in the phenylacetylene oxidation chemistry remains large and should be addressed in future studies.

Finally, Fig. 6 reports the mean widths of confidence intervals for the true mean deviation factors for a $C = 90\%$ confidence level. For the relatively accurate prediction of C_5H_6, C_6H_6, A_1CH_3, and $A_1C_2H_3$ peak mole fractions, the average lower interval bound is close to one, indicating that the estimated mean error is of a similar magnitude as its uncertainty. Increasing the assumed sample size n from 2 to 5 for constant standard deviation would reduce the width of the confidence intervals by a factor of $\sim$2, highlighting the benefit of a larger sample size. For the other less accurately predicted species, the effects of uncertainty in the measurements are small compared to the mean error in the model predictions.

4. Reaction flux analysis

Reaction flux analysis or reaction path analysis is commonly used in chemical kinetic model development studies. Reaction flux diagrams visualize pathways that consume or produce species of interest, which helps understand a chemical kinetic model. The key information conveyed in these diagrams is the distinction between shown "significant" and discarded "insignificant" pathways. However, despite the complexity of detailed chemical kinetic models and the strong reduction of the information expressed in a flux diagram, most studies do not define selection criteria for shown species and fluxes rigorously. Additionally, in the case of manually assembled diagrams, species or flux selection is error-prone and can be inconsistent unless the diagram is sufficiently simple. In contrast, this paper introduces a graph model based on net reaction fluxes defining rigorous selection criteria for the shown species and fluxes, enabling the automatic generation of flux diagrams. The details of the selection process are described in Appendix A.

Briefly, the construction process of a flux diagram is based on net reaction fluxes and the definition of a set of source and target species. The species of interest, indene, naphthalene, or $C_{12}H_8$ isomers in the present work, are the target species. Additionally, the Supplementary Material includes analyses for benzene. As significant formation pathways are to be discovered by the analyses, all species in the model with four or more carbon atoms define the set of source species. A two-step process identifies the visualized pathways, where reaction fluxes along shown pathways connecting a source and a target species must fulfill a constraining criterion. The first step determines significant pathways producing a target i using a cut-off parameter P_i defined in Eq. (A.2). Pathways fulfilling the criterion are shown with solid arrows. The second step adds dashed arrows representing reaction fluxes explaining interactions between pathways from the first step and cycles based on a global cut-off parameter p_{limit} defined in Eq. (A.6).

This graph-based representation of the reaction fluxes will be used in the following to generate flux diagrams from simulation results. The selection of fluxes and species is rigorous, and all information shown in the flux diagrams is quantitative, making only the selection of target species and the chosen cut-off parameter values subjective.

4.1. Indene

The pathways contributing significantly to the indene formation are largely similar for all considered counterflow flames, exhibiting moderate dependence on mixture composition, pressure, and fuel structure. The diagram in Fig. 7 is representative of the fluxes observed in most of the investigated flames. It shows three major indene formation pathways.

The first indene (C_9H_8) formation pathway belongs to the naphthalene oxidation chemistry. The pathway depicted in Fig. 7 starts from 1-naphthyl radical (A_2-A) oxidation, which proceeds via naphthoxy (A_2O) and indenyl (C_9H_7) formation. Several 1-naphthyl oxidation reactions can significantly contribute to the naphthoxy formation, where reactions and rate coefficients were taken by analogy to reactions of phenyl [132]. The subsequent naphthoxy radical decomposition is assumed to proceed analogously to phenoxy decomposition [150]. Kislov et al. [270] investigated the products produced from naphthyl oxidation, and their results indicate that the product selection for these reactions by analogy to phenyl reactions is plausible. However, the uncertainty in estimated rate parameters and product branching remains considerable, potentially contributing to the overprediction of indene shown in Fig. 6. A revision of the naphthalene oxidation chemistry emphasizing indene formation pathways should be the subject of future studies.

The second group of pathways shown in Fig. 7 starts from benzene (A_1). H-abstraction of benzene produces phenyl, and the subsequent recombination of phenyl (A_1-) and propargyl (C_3H_3) initiates several growth pathways, primarily via aliphatic C_9H_8 isomers, where the dominant pathway depends on the considered conditions. Direct indenyl radical formation [145] can be a significant pathway. However, direct indene formation, which is one of the reactions investigated by Morozov et al. [175], is insignificant in the considered flames. In partially premixed ethylene/oxygen/nitrogen counterflow flames, investigated experimentally by Carbone et al. [230], the reaction of phenylacetylene (A_1C_2H) and methyl [145] can contribute to the formation of aliphatic C_9H_8 isomers. Phenylacetylene, in turn, is produced from the first step of Frenklach's original HACA route, which is usually thought of as a naphthalene formation pathway [146].

In contrast to the naphthalene oxidation pathways, the subset of pressure-dependent reactions starting from benzene is based on theoretical calculations by Mebel and co-workers [145,146,175]. The associated uncertainty is considerably smaller than for the naphthalene oxidation pathways. Additionally, this subset of reactions was shown to contribute to the indene formation when integrated into other chemical kinetic models [35,36]. Therefore, we can confidently state that this subset of reactions is a viable pathway that contributes significantly to the indene formation in a broad range of conditions and for several fuels. The subset should be considered in chemical kinetic models for PAH growth.

The third indene-producing pathway shown in Fig. 7 is acetylene addition to benzyl radicals (A_1CH_2) [145]. This pathway can be initiated by reactions of methyl and phenyl radicals [271], as shown in Fig. 7. However, significant indene formation is possible via this pathway without phenyl radical formation, for example,

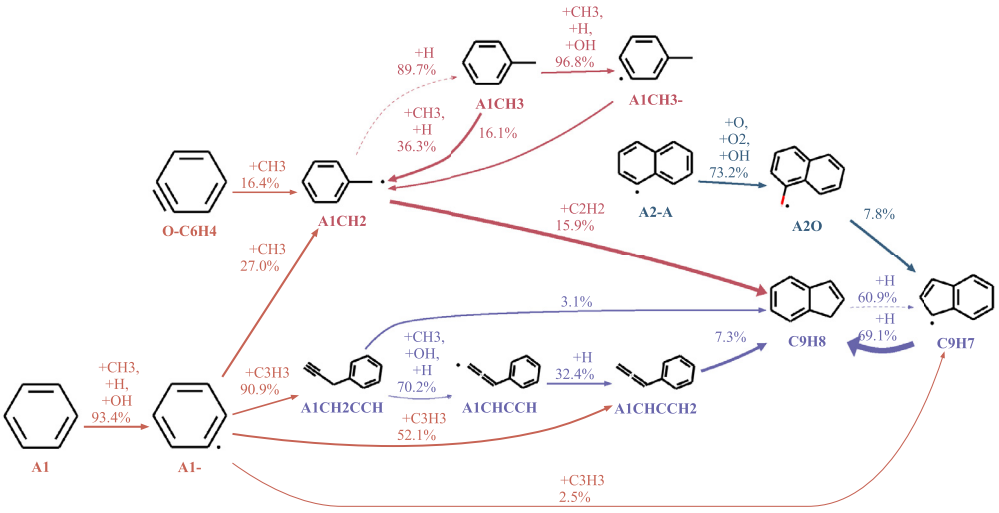

Fig. 7. Indene formation pathways ($P_{C9H8} = 1.6\%$, $p_{limit} = 35\%$) in an atmospheric acetylene/oxygen/argon/carbon dioxide counterflow diffusion flame experimentally investigated by Baroncelli et al. [227]. Figure S26 shows a detailed comparison of measured and computed species mole fractions and the boundary conditions. Vertex labels show the species names used in the developed chemical kinetic model. Edge labels show relative contributions of a pathway to a species' integrated production flux and further reactants consumed in the associated reactions. The linewidth of solid arrows represents the significance of a pathway for a target's formation as defined in Appendix A. Pathways shown with dashed arrows explain interactions between pathways or cycles. Colors represent the number of carbon atoms in the species.

from reactions of benzyne ($O\text{-}C_6H_4$) and methyl radicals [111]. Interestingly, Hansen et al. [36] found minor contributions from this pathway when investigating premixed propyne-doped benzene and toluene flames. The benzyl pathway is often the dominant indene formation route for the counterflow flames considered in the present work. Both chemical kinetic models use the same subset of reactions proposed by Mebel et al. [145]. The cause for the deviating dominant formation routes remains to be investigated.

Reactions with cyclopentadiene [176] can play a minor role in the indene formation, as, for example, observed in the low-pressure cyclopentene flames investigated by Baroncelli et al. [133]. Another minor contributor to the indenyl radical formation is the reaction of benzyne and propargyl radicals [178].

4.2. Naphthalene

The dominant naphthalene formation pathways depend more strongly than indene formation pathways on the fuel composition, so naphthalene production flux analysis is discussed with the help of three examples. The examples were selected to cover significant naphthalene pathways from all considered flames.

Figure 8 shows the naphthalene formation pathways in an atmospheric, argon-diluted acetylene flame investigated experimentally by Baroncelli et al. [227]. The shown relative flux contributions to naphthalene (A_2) sum up to 25.7% because cyclic pathways with naphthyl radicals making up 70% of the flux are not shown for clarity. As for indene, multiple pathways initiated by reactions of benzene (A_1) can play an essential role. Three HACA pathways contribute to the naphthalene formation in this acetylene flame. The first contributor is Frenklach's original HACA route [146], which proceeds via phenylacetylene (A_1C_2H). Second, the similar pathway from the model of Chu et al. [56] is of comparable significance. Dehydrogenated $C_{10}H_7$ intermediates in these pathways were omitted for clarity. Third, the Bittner–Howard HACA route [146], in which a second acetylene molecule adds to the styryl radical A_1CHCH, is non-negligible. The modified Frenklach HACA route [146] is negligible in this atmospheric pressure flame. At higher pressures, the modified Frenklach and the Bittner–Howard route are expected to become more significant than the HACA routes proceeding via phenylacetylene [146]. However, HACA routes constitute a non-negligible naphthalene formation pathway only in acetylene flames, and only atmospheric acetylene flames were considered.

Minor or negligible contributions to the naphthalene formation from HACA routes can be surprising as HACA is often expected to be an important route from benzene to naphthalene [182]. Directly measured products formed from phenyl + acetylene at up to 0.4 bar pressure and temperatures up to 1020 K showed that viable pathways connecting the two species exist [181,182]. The HACA reaction kinetics in the developed model were derived from theoretical calculations [56,146,182] and predicted species concentrations mostly in agreement with direct measurements [56,182]. However, recent chemical kinetic modeling studies of non-premixed [35] and premixed flames [36] using the reaction kinetics of Mebel et al. [146] questioned the importance of HACA pathways. Naphthalene formation was dominated by radical–radical and, to a lesser extent, ring-enlargement reactions [35,36], even when benzene was the fuel [36]. Predictions of the model developed in the present work confirm the minor contributions from HACA pathways and highlight the importance of radical–radical and PAH molecule–radical reactions for naphthalene formation.

As shown in Fig. 8, the reaction of benzene (A_1) and the resonantly stabilized free radical $i\text{-}C_4H_3$ is predicted to be a naphthalene-producing reaction of significance. The used rate coefficient is an estimate for reactions between molecules and resonantly stabilized radicals adopted from the model of Pejpichestakul et al. [10]. With this estimate [10], the reaction significantly contributes to naphthalene formation in several other flames. A more accurate rate coefficient, e.g., derived from theoretical calculations, would be appropriate, but, to the authors' knowledge, it is unavailable in the literature. As an alternative to the currently adopted estimate [10], the analogy with $A_1 + C_3H_3$ [145] can be considered. This analogy suggests a significantly lower rate coefficient and the possibility of forming one-ring species with an aliphatic substitute that might be converted to naphthalene. Using the analogy with $A_1 + C_3H_3$ [145], contributions from the reaction $A_1 + i\text{-}C_4H_3$ to the naphthalene formation become negligible in all considered counterflow flames. The resulting parity diagrams are included in the Supplementary Material. The mean deviation factor for the $C_{10}H_8$ peak species mole fractions decreases slightly from 2.28 to 2.08.

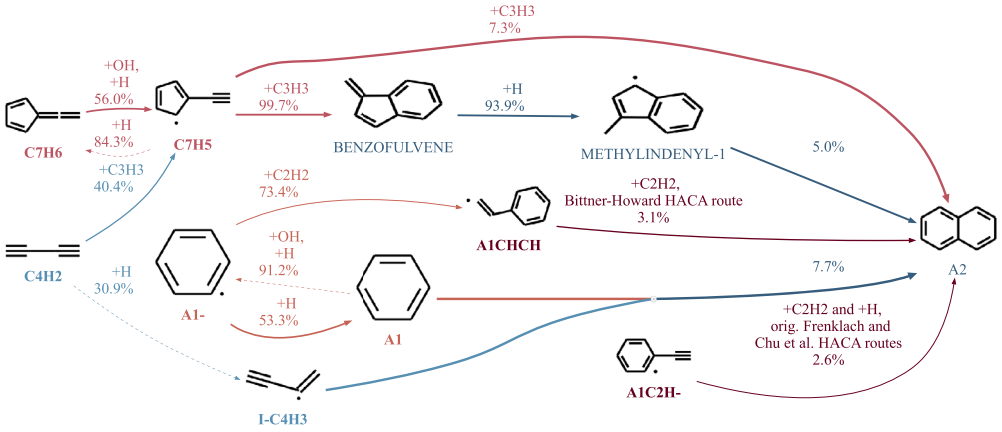

Fig. 8. Naphthalene formation pathways ($P_{A2} = 2.1\%$, $p_{limit} = 30\%$, and source species are species with 4–9 carbon atoms) in an atmospheric acetylene/oxygen/argon diffusion flame experimentally investigated by Baroncelli et al. [227]. Figure S25 shows a detailed comparison of measured and computed species mole fractions and the boundary conditions. The meaning of labels, line types, linewidth, and colors is the same as in Fig. 7. The dot that connects A_1 and i-C_4H_3 represents a reaction.

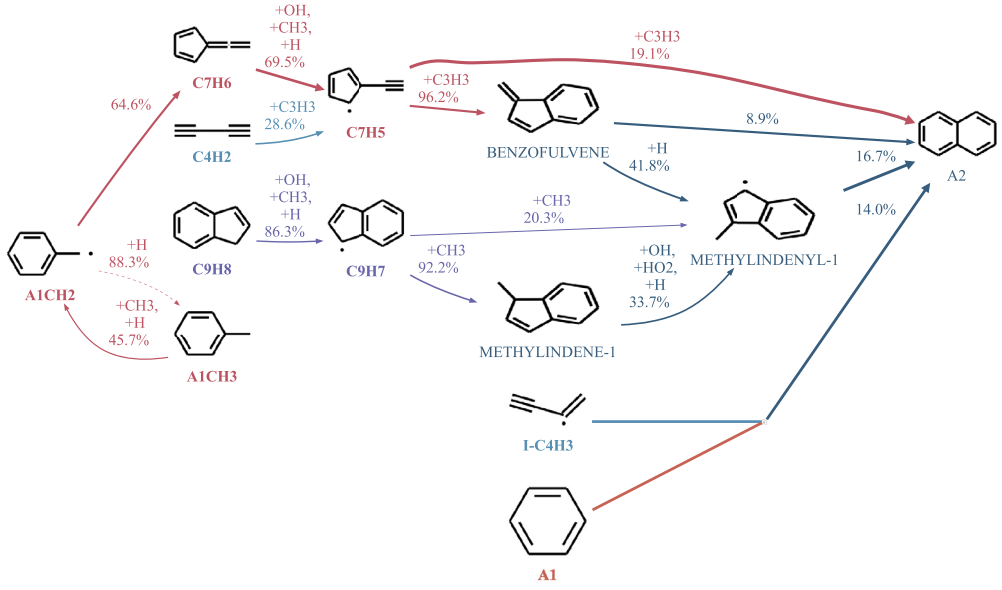

Fig. 9. Naphthalene formation pathways ($P_{A2} = 3.2\%$ and $p_{limit} = 80\%$, and source species are species with 4–9 carbon atoms) in a partially premixed ethylene/oxygen/nitrogen flame at 4 atm experimentally investigated by Carbone et al. [230]. Figure S32 shows a detailed comparison of measured and computed species mole fractions and the boundary conditions. Pathways were clipped for species with four carbon atoms. The meaning of labels, line types, linewidth, and colors is the same as in Fig. 7. The dot that connects A_1 and i-C_4H_3 represents a reaction.

Given the high uncertainty in the proposed pathway and the employed estimate, future studies should revisit this reaction once more reliable reaction kinetics are available.

Fulvenallenyl radical (C_7H_5) pathways contribute significantly to naphthalene formation in several flames, including the acetylene flame analyzed in Fig. 8. Following Kukkadapu et al. [35], fulvenallenyl and propargyl recombination reactions can produce naphthalene or benzofulvene. Benzofulvene is subsequently directly or, as shown in Fig. 8, indirectly [145] converted to naphthalene. Contributions from these reactions are similar to other pathways for the acetylene counterflow flame analyzed in Fig. 8. However, this pathway dominates the naphthalene formation in many other flames. Kukkadapu and co-workers [35,36,109] also ascertained the importance of this pathway, and we agree that it would be recommended to study this reaction theoretically.

Figure 9 shows the production flux of naphthalene in a partially premixed ethylene/oxygen/nitrogen flame at a pressure of 4 atm. In contrast to the acetylene flame, the fulvenallenyl radical pathways are responsible for most of the naphthalene formation. As shown in Fig. 9, fulvenallenyl radicals (C_7H_5) are produced in two ways.

First, propargyl can react with diacetylene (C_4H_2) to form fulvenallenyl [111,113]. This reaction is prototypical for an H-elimination/abstraction-free PAH growth mechanism [113] and should receive further attention in future studies. Diacetylene chemistry is poorly understood, and an overprediction was observed in many of the considered flames, including the partially premixed ethylene/oxygen/nitrogen flame analyzed in Fig. 9. This overprediction could promote the emergence of fulvenallenyl radical pathways, potentially overestimating their significance. Pejpichestakul et al. [10] investigated PAH formation in several rich premixed flames, and they share the conclusion that diacetylene deserves attention in future studies. Second, the dehydrogenation of the benzyl radicals (A_1CH_2) can produce fulvenallenyl radicals [110,111]. As shown in Fig. 9, another pathway contributing significantly to the naphthalene formation is the reaction of benzene and i-C_4H_3, which has been discussed above.

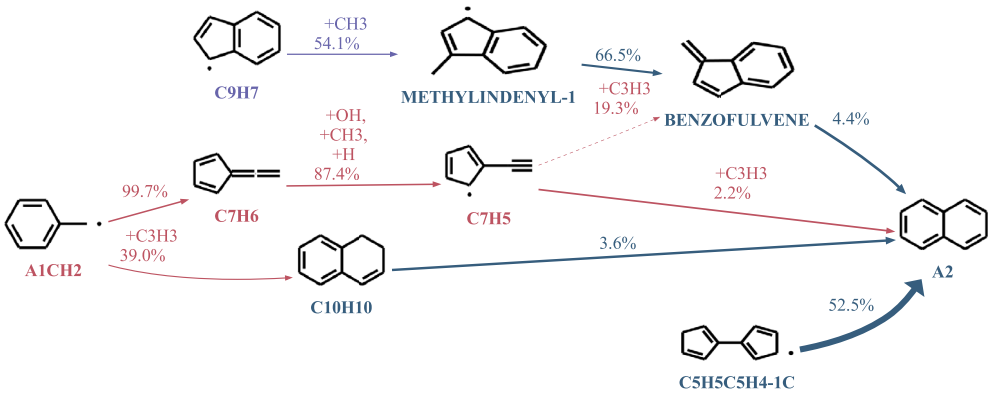

Fig. 10. Naphthalene formation pathways (P_{A2} = 1.3% and p_{limit} = 10%) in a methane-doped low-pressure cyclopentene/oxygen/argon at 80 mbar experimentally investigated by Baroncelli et al. [133]. Figure S76 shows a detailed comparison of measured and computed species mole fractions and the boundary conditions. Formation pathways of $C_5H_5C_5H_4$-1C are part of a complex network initiated by recombination reactions of cyclopentadienyl radicals [135] and were clipped. Cyclic pathways with naphthyl radicals are excluded for clarity. The meaning of labels, line types, linewidth, and colors is the same as in Fig. 7.

Finally, naphthalene formation can also be initiated by the recombination reaction of methyl and indenyl radicals (C_9H_7). Such molecular growth reactions through ring-enlargement were found to be significant naphthalene formation pathways by Kukkadapu and co-workers [35,36,109]. However, for the considered counterflow flames, these pathways were minor contributors.

The reaction fluxes for naphthalene production in a methane-doped low-pressure cyclopentene/argon/oxygen flame [133] are summarized in Fig. 10. The primary source of naphthalene is here an H-elimination reaction of the fulvalanyl radical $C_5H_5C_5H_4$-1C, which is produced from a complex pressure-dependent reaction network proposed by Long et al. [135]. The initiation reactions of the network are recombination reactions of cyclopentadienyl radicals (C_5H_5). Rate coefficients for the cyclopentadienyl recombination reactions were reduced by a factor of four to match the experimental measurements.

Additionally, Fig. 10 shows three minor pathways, the indenyl ring-enlargement pathway starting from C_9H_7, the fulvenallenyl (C_7H_5) pathway, and the naphthalene formation from dialin ($C_{10}H_{10}$). Dialin is produced from the recombination of benzyl and propargyl radicals. Other products of the benzyl-propargyl recombination, such as phenyl-vinylacetylenes, are considered in the developed model. Following the model of Kukkaduppa et al. [35], these reactions can initiate a complex reaction sequence that can contribute to naphthalene formation [36]. However, the adopted subset had a negligible effect on naphthalene formation for the considered counterflow flames.

4.3. Acenaphthalene and ethynylnaphthalenes

Figure 11 shows an acenaphthalene (A_2R_5) production flux analysis for a partially premixed ethylene/oxygen/nitrogen flame at atmospheric pressure. It reveals that acenaphthalene is almost exclusively produced from acetylene addition to 1-naphthyl radicals (A_2-A). These reactions belong to the HACA routes included in Chu et al.'s detailed chemical kinetic model [56]. HACA pathways dominate the formation of $C_{12}H_8$ isomers in most of the considered flames, although propyne addition to 1-naphthyl can be a minor contributor. At high pressures, assumed products of phenanthrene oxidation reactions can produce significant amounts of ethynylnaphthalenes. The analysis below focuses on the flames unaffected by this highly uncertain oxidation pathway.

In contrast to the model of Cai et al. [62], the dominant formation pathways in the $C_{12}H_8$ chemistry shown in Fig. 11 are based on theoretical calculations [55,56]. The adopted detailed description [56] allows for an analysis of the predicted $C_{12}H_8$ isomer distribution. Besides its relevance for possible PAH growth pathways, the isomer distribution is of interest for quantifying mole fractions from experimental measurements [243] or determining the properties of lumped species [10]. The high thermodynamic stability of acenaphthalene is well known [194,195]. Using group additivity estimates and considering mixtures of acetylene, molecular hydrogen, and one of the $C_{12}H_8$ isomers, the hypothetical equilibrium concentration of acenaphthalene at 1800 K was shown to be 40 times larger than that of 1-ethynylnaphthalene (A_2C_2HA) [194]. Based on this simple thermodynamic analysis, one would expect that acenaphthalene is the most abundant $C_{12}H_8$ isomer. Figure 12 shows that mole fractions of the 1-ethynylnaphthalene, 2-ethynylnaphthalene, and acenaphthalene are predicted to be similarly large for the considered flame. Model predictions from the comparison to experimental measurements in the Supplementary Material suggest that a more or less even distribution among these three isomers can be expected in many flames. Other $C_{12}H_8$ isomers adopted from the detailed model of Chu et al. [56] are only present in negligible concentrations. The observed $C_{12}H_8$ isomer distribution distinguishes itself from $C_{10}H_8$ and C_9H_8 isomer distributions, where naphthalene and indene are the most abundant species.

The reaction flux analysis shown in Fig. 11 explains the high concentration of ethynylnaphthalenes. First, 2-ethynylnaphthalene (A_2C_2HB) is produced in the acetylene addition to a 2-naphthyl radical (A_2-B). Subsequently, no significant pathway allows for the conversion of 2-ethynylnaphthalene to 1-ethynylnaphthalene (A_2C_2HA) or acenaphthalene [56]. As reported by Liu et al. [54] and included in the present model, the Frenklach pathway of 2-ethynylnaphthalene can potentially produce phenanthrene and anthracene. However, experimental [50] and theoretical [54,56] evidence shows that HACA pathways are unlikely to produce significant amounts of three-ring $C_{14}H_{10}$ species. Instead, the di-substituted $C_{14}H_8$ isomers are the favorable product [56] of the acetylene addition reactions. Accordingly, the model predicts insignificant contributions to the phenanthrene formation via HACA routes.

The 1-ethynylnaphthalene (A_2C_2HA) mole fraction being similar to the acenaphthalene mole fraction, as exemplified by Fig. 12, is surprising given the thermodynamic stability of acenaphthalene and the kinetic analysis of Liu et al. [54] that showed that the formation of acenaphthalene from 1-naphthyl radicals (A_2-A) is favorable over the formation of 1-ethynylnaphthalene. In addition to the work of Liu et al. [54], the developed kinetic model incorporates the reaction network of Chu et al. [56], who computed rate coefficients for the reaction between N1-CS12 and N1-CS41,

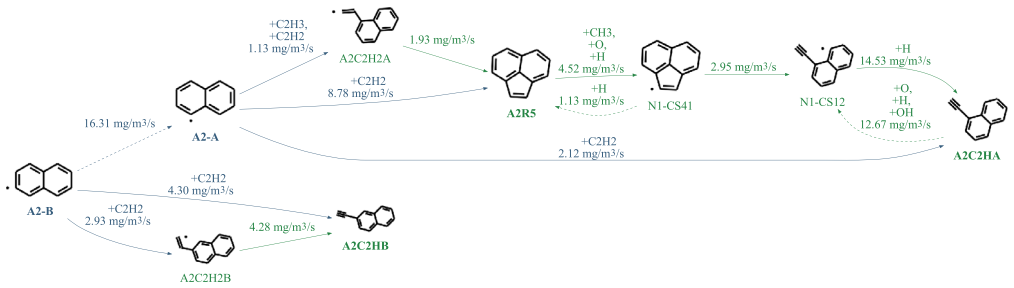

Fig. 11. Formations pathways of acenaphthalene ($P_{A2R5} = 2\%$), 1-ethynylnaphthalene ($P_{A2C2HA} = 0.8\%$), and 2-ethynylnaphthalene ($P_{A2C2HB} = 2\%$) in an atmospheric partially premixed ethylene/oxygen/nitrogen flame for $p_{limit} = 3\%$. Source species are A_2R_5, A_2C_2HA, A_2C_2HB, and all species with 4 to 10 carbon atoms. A uniform linewidth is used for the significant pathways (solid lines), and edge labels show absolute integrated production fluxes. Figure S29 shows a detailed comparison of measured and computed species mole fractions and the boundary conditions.

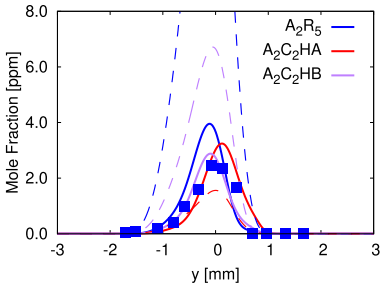

Fig. 12. Species mole fractions of acenaphthalene (A_2R_5), 1-ethynylnaphthalene (A_2C_2HA), and 2-ethynylnaphthalene (A_2C_2HB) as a function of distance from the stagnation plane for the ethylene/oxygen/nitrogen flame analyzed in Fig. 11. Symbols show experimental measurements of the A_2R_5 mole fraction by Carbone et al. [230]. Solid lines show predictions of the model developed in the present work, and dashed lines show predictions of the model of Cai et al. [62].

which constitutes an isomerization via direct intramolecular H-transfer. Figure 11 shows that, as expected [54], acetylene addition to 1-naphthyl radicals produces predominantly acenaphthalene. However, significant amounts of 1-ethynylnaphthalene can be produced via the isomerization reaction investigated by Chu et al. [56], slightly lowering the acenaphthalene mole fraction. As for 2-ethynylnaphthalene, there is an insignificant reaction flux in the reverse direction from 1-ethynylnaphthalene to acenaphthalene.

While the reaction flux analysis in Fig. 11 shows that a significant reaction flux between $C_{12}H_8$ isomers is possible, the uncertainty in the isomer distributions shown in Fig. 12 is substantial. Consumption pathways, for example, through oxidation, are currently of minor importance. However, the developed model uses relatively crude estimates following prior works [36,62], which could affect the predictions.

5. Conclusion

This study develops a new detailed chemical kinetic model for predicting PAH species up to the size of acepyrene. The developed model reflects the latest understanding of PAH chemistry informed by ab-initio, experimental, and chemical kinetic model development studies. The chemistry of soot precursors, including C_3H_4 isomers, C_4H_6 isomers, cyclopentadiene, benzene, substituted monoaromatic species, indene, naphthalene, $C_{12}H_8$ isomers, and phenanthrene, was updated starting from the model of Cai et al. [62] for gasoline surrogates.

The model was validated against measurements from 79 experimental studies, including ignition delay times, laminar burning velocities, and speciation data, for several fuels in various conditions. Prediction errors for oxidation chemistry validation targets were overall similar for the proposed model and the model of Cai et al. [62]. The PAH chemistry was validated against measured peak mole fractions of aromatic species from 31 counterflow flames. The predictions improved significantly compared to the model of Cai et al. [62]. Mean deviations between computed and measured peak mole fractions of selected aromatic species up the size of acenaphthalene were below a factor of three.

Computing confidence intervals quantified the effects of experimental uncertainties for a 90% confidence level. The confidence intervals' mean width is similarly large as the mean prediction error of simple aromatic species. A larger sample size, that is, a larger number of conducted measurements at the same conditions, would achieve a significant width reduction. The experimental uncertainties are of minor significance for assessing the model prediction errors in mole fractions of two- and three-ring aromatic species.

Reaction flux analyses applying rigorously defined species selection criteria revealed the dominant formation pathways of indene, naphthalene, and acenaphthalene. The analysis of indene highlights the importance of formation pathways initialized by reactions of phenyl and benzyl, which are described by the pressure-dependent reaction kinetics from high-level quantum chemistry calculations [138,145,175].

The reaction flux analysis of naphthalene revealed that the two most significant formation pathways are highly uncertain for the following reasons:

1. The reaction A_1 + i-C_4H_3 $\rightleftharpoons$ A_2 + H contributes significantly to the naphthalene formation, where the rate coefficient estimate was adopted from Pejpichestakul et al. [10]. An alternative estimation approach based on the analogy with A_1 + C_3H_3 [145] suggests a lower rate coefficient resulting in negligible contributions to the naphthalene formation. The pathway should be revisited once more reliable reaction kinetics are available.
2. The analysis confirmed the previously observed [35,36,109] significance of fulvenallenyl radical pathways. The recombination reactions of fulvenallenyl and propargyl are taken by analogy to the recombination reactions of propargyl radicals.
3. An essential precursor of fulvenallenyl, diacetylene, is strongly overpredicted in many flames, reflecting the considerable uncertainty in predictions of C_4 species.

HACA routes [66,146,182] and ring-enlargement pathways [185] are minor contributors or negligible. Cyclopentadienyl recombination [135] is the dominant pathway in cyclopentene flames but negligible for other fuels.

Acenaphthalene is produced from naphthalene via HACA routes. The model predictions suggest that the 1-ethynylnaphthalene and 2-ethynylnaphthalene concentrations are often similar to the acenaphthalene concentrations.

Future studies should address the uncertainties in the naphthalene formation pathways and the significant uncertainties in the oxidation of phenylacetylene, indene, naphthalene, and larger PAH species.

Declaration of Competing Interest

The authors declare that they have no known competing financial interests or personal relationships that could have appeared to influence the work reported in this paper.

Acknowledgments

The authors thank Stephen J. Klippenstein, Argonne Distinguished Fellow, for the enlightening discussions and insights.

We would like to acknowledge the financial support of the CRG project under project number URF/1/4688-01-01 funded by KAUST.

Appendix A. Selection criteria for species and reactions in reaction flux diagrams

The graph model for the flux analysis is a bipartite graph, where the two parts are the set of species $\mathcal{S}$ and the set of reactions $\mathcal{R}$. The edges represent the integrated net reaction fluxes. The graph is directed where the direction coincides with the direction of the net reaction rate for consumption pathway analysis or vice versa for formation pathway analysis. Starting from a set of chosen species of interest, referred to as target species, $\mathcal{S}_T$, all traversable paths in the graph contribute directly or indirectly to the consumption or formation of a target species. However, it is unclear which paths are the most relevant, and their number will usually be too large to depict all of them in a flux diagram. Therefore, the pathways shown in a flux diagram are further constrained by introducing a set of source species $\mathcal{S}_S$ and requiring that every shown pathway satisfies a selection criterion that asserts a significant reaction flux between a target and a source species. Consider an acyclic pathway candidate w that joins the vertice sequence

$$\nu_w = (S_1, R_1, S_2, \ldots, R_{n-2}, S_{n-1}, R_{n-1}, S_n), \tag{A.1}$$

with $S_1 \in \mathcal{S}_S$, $S_n \in \mathcal{S}_T$, $S_1, \ldots, S_n \in \mathcal{S}$, and $R_1, \ldots, R_{n-1} \in \mathcal{R}$. For w to be shown in a production flux diagram, it must satisfy the condition

$$P_{S_n} < \prod_{i=1}^{n-1} p_{S_i,S_{i+1}}, \tag{A.2}$$

where P_{S_n} is the chosen cut-off parameter for a target species S_n, $p_{S_i,S_{i+1}}$ is an interaction coefficient for the S_{i+1} producing and S_i consuming reactions given by

$$p_{S_i,S_{i+1}} = \frac{\sum_{j\in N(S_i,S_{i+1})} \max\left(0, \int \nu_{j,S_{i+1}}\omega_j \mathrm{d}x\right)}{\sum_{j=1}^{n_\mathrm{R}} \max\left(0, \int \nu_{j,S_{i+1}}\omega_j \mathrm{d}x\right)}, \tag{A.3}$$

ω_j is the net reaction rate of reaction j, $\nu_{j,S_{i+1}}$ is the net stoichiometric coefficient of species S_{i+1} in the reaction j, n_R is the number of reactions, and dx represents the appropriate integration in time or space. The sum over all reactions adjacent to the species pair, indicated by $N(S_i, S_{i+1})$, is used because multiple reactions connecting the two species are merged in the flux diagram. An example of such a group is the H-abstraction of S_i by several radicals producing the respective radical S_{i+1}. Analogously, a consumption flux diagram shows a pathway that consumes the target species S_n if

$$C_{S_n} < \prod_{i=1}^{n-1} c_{S_i,S_{i+1}}, \tag{A.4}$$

where

$$c_{S_i,S_{i+1}} = \frac{\sum_{j\in N(S_i,S_{i+1})} \max\left(0, \int -\nu_{j,S_{i+1}}\omega_j \mathrm{d}x\right)}{\sum_{j=1}^{n_\mathrm{R}} \max\left(0, \int -\nu_{j,S_{i+1}}\omega_j \mathrm{d}x\right)}. \tag{A.5}$$

The respective criterion is tested for every possible pathway in the graph without visiting any vertex twice. All flux diagrams depict pathways fulfilling the minimum flux criterion with solid arrows. The linewidth of an arrow depicting an edge increases with larger values of the respective flux criterion in Eqs. (A.2) and (A.4) if the flux analysis is done for a single target species. Labels next to edges show reactants enabling the visualized flux and the relative flux contributions to a species as given by Eqs. (A.3) and (A.5). The final step adds further pathways that explain interactions between already shown pathways and cycles. These additional pathways must not add additional vertices. A pathway candidate joining (S_i, R, S_j) is shown if

$$p_{S_i,S_j} > p_\mathrm{limit} \tag{A.6}$$

for production flux analysis or

$$c_{S_i,S_j} > c_\mathrm{limit} \tag{A.7}$$

for consumption flux analysis, where p_limit and c_limit are global cut-off parameters for a diagram. Pathways added in the second step are depicted with dashed lines of uniform linewidth. Both types of edges and the vertex labels are color-coded according to the number of carbon atoms in the species. The set of source species is defined as the set of species with four or more carbon atoms unless otherwise stated, and source species are marked in bold.

Supplementary material

Supplementary material associated with this article can be found, in the online version, at doi:10.1016/j.combustflame.2022.112574.

References

[1] C.-E. Boström, P. Gerde, A. Hanberg, B. Jernström, C. Johansson, T. Kyrklund, A. Rannug, M. Törnqvist, K. Victorin, R. Westerholm, Cancer risk assessment, indicators, and guidelines for polycyclic aromatic hydrocarbons in the ambient air, Environ. Health Perspect. 110 (suppl 3) (2002) 451–488, doi:10.1289/ehp.110-1241197.

[2] B. Kumfer, I. Kennedy, The role of soot in the health effects of inhaled airborne particles, in: B. Bockhorn, A. D'Anna, A. Sarofim, H. Wang (Eds.), Combustion Generated fine Carbonaceous Particles, KIT Scientific Publishing, Karlsruhe, Germany (2009), pp. 1–15, doi:10.5445/KSP/1000013744.

[3] C.S. McEnally, L.D. Pfefferle, B. Atakan, K. Kohse-Höinghaus, Studies of aromatic hydrocarbon formation mechanisms in flames: progress towards closing the fuel gap, Prog. Energy Combust. Sci. 32 (3) (2006) 247–294, doi:10.1016/j.pecs.2005.11.003.

[4] M.Z. Jacobson, Strong radiative heating due to the mixing state of black carbon in atmospheric aerosols, Nature 409 (6821) (2001) 695–697, doi:10.1038/35055518.

[5] K. Adachi, S.H. Chung, P.R. Buseck, Shapes of soot aerosol particles and implications for their effects on climate, J. Geophys. Res. 115 (D15206) (2010), doi:10.1029/2009JD012868.

[6] D. Shindell, J.C.I. Kuylenstierna, E. Vignati, R. van Dingenen, M. Amann, Z. Klimont, S.C. Anenberg, N. Muller, G. Janssens-Maenhout, F. Raes, J. Schwartz, G. Faluvegi, L. Pozzoli, K. Kupiainen, L. Höglund-Isaksson, L. Emberson, D. Streets, V. Ramanathan, K. Hicks, N.T.K. Oanh, G. Milly, M. Williams, V. Demkine, D. Fowler, Simultaneously mitigating near-term climate change and improving human health and food security, Science 335 (6065) (2012) 183–189, doi:10.1126/science.1210026.

[7] D. Shindell, G. Faluvegi, M. Walsh, S.C. Anenberg, R. Van Dingenen, N.Z. Muller, J. Austin, D. Koch, G. Milly, Climate, health, agricultural and economic impacts of tighter vehicle-emission standards, Nat. Clim. Change 1 (1) (2011) 59–66, doi:10.1038/nclimate1066.

[8] J. Appel, H. Bockhorn, M. Frenklach, Kinetic modeling of soot formation with detailed chemistry and physics: laminar premixed flames of C_2 hydrocarbons, Combust. Flame 121 (1) (2000) 122–136, doi:10.1016/S0010-2180(99)00135-2.

[9] G. Blanquart, H. Pitsch, A joint volume-surface-hydrogen multi-variate model for soot formation, in: B. Bockhorn, A. D'Anna, A. Sarofim, H. Wang (Eds.), Combustion Generated Fine Carbonaceous Particles, KIT Scientific Publishing, Karlsruhe, Germany (2009), pp. 437–463, doi:10.5445/KSP/1000013744.

[10] W. Pejpichestakul, E. Ranzi, M. Pelucchi, A. Frassoldati, A. Cuoci, A. Parente, T. Faravelli, Examination of a soot model in premixed laminar flames at fuel-rich conditions, Proc. Combust. Inst. 37 (1) (2019) 1013–1021, doi:10.1016/j.proci.2018.06.104.
[11] A. Nobili, L. Pratali Maffei, A. Baggioli, M. Pelucchi, A. Cuoci, C. Cavallotti, T. Faravelli, On the radical behavior of large polycyclic aromatic hydrocarbons in soot formation and oxidation, Combust. Flame 235 (2022) 111692.
[12] A. Nobili, W. Pejpichestakul, M. Pelucchi, A. Cuoci, C. Cavallotti, T. Faravelli, Modeling soot particles as stable radicals: a chemical kinetic study on formation and oxidation. Part II. Soot oxidation in flow reactors and laminar flames, Combust. Flame (2022) 112072, doi:10.1016/j.combustflame.2022.112072.
[13] A. Nobili, A. Cuoci, W. Pejpichestakul, M. Pelucchi, C. Cavallotti, T. Faravelli, Modeling soot particles as stable radicals: a chemical kinetic study on formation and oxidation. Part I. Soot formation in ethylene laminar premixed and counterflow diffusion flames, Combust. Flame (2022) 112073, doi:10.1016/j.combustflame.2022.112073.
[14] H. Wang, Formation of nascent soot and other condensed-phase materials in flames, Proc. Combust. Inst. 33 (1) (2011) 41–67, doi:10.1016/j.proci.2010.09.009.
[15] M. Frenklach, Reaction mechanism of soot formation in flames, Phys. Chem. Chem. Phys. 4 (2002) 2028–2037, doi:10.1039/B110045A.
[16] P. Lindstedt, L. Maurice, M. Meyer, Thermodynamic and kinetic issues in the formation and oxidation of aromatic species, Faraday Discuss. 119 (2002) 409–432, doi:10.1039/B104056C.
[17] M.J. Castaldi, N.M. Marinov, C.F. Melius, J. Huang, S.M. Senkan, W.J. Pit, C.K. Westbrook, Experimental and modeling investigation of aromatic and polycyclic aromatic hydrocarbon formation in a premixed ethylene flame, Symp. (Int.) Combust. 26 (1) (1996) 693–702, doi:10.1016/S0082-0784(96)80277-3.
[18] N.M. Marinov, W.J. Pitz, C.K. Westbrook, M.J. Castaldi, S.M. Senkan, Modeling of aromatic and polycyclic aromatic hydrocarbon formation in premixed methane and ethane flames, Combust. Sci. Technol. 116–117 (1–6) (1996) 211–287, doi:10.1080/00102209608935550.
[19] H. Richter, W.J. Grieco, J.B. Howard, Formation mechanism of polycyclic aromatic hydrocarbons and fullerenes in premixed benzene flames, Combust. Flame 119 (1) (1999) 1–22, doi:10.1016/S0010-2180(99)00032-2.
[20] N.M. Marinov, W.J. Pitz, C.K. Westbrook, A.M. Vincitore, M.J. Castaldi, S.M. Senkan, C.F. Melius, Aromatic and polycyclic aromatic hydrocarbon formation in a laminar premixed *n*-butane flame, Combust. Flame 114 (1) (1998) 192–213, doi:10.1016/S0010-2180(97)00275-7.
[21] S. Granata, T. Faravelli, E. Ranzi, N. Olten, S. Senkan, Kinetic modeling of counterflow diffusion flames of butadiene, Combust. Flame 131 (3) (2002) 273–284, doi:10.1016/S0010-2180(02)00407-8.
[22] M. Frenklach, H. Wang, Detailed modeling of soot particle nucleation and growth, Symp. (Int.) Combust. 23 (1) (1991) 1559–1566, doi:10.1016/S0082-0784(06)80426-1.
[23] V.V. Kislov, N.I. Islamova, A.M. Kolker, S.H. Lin, A.M. Mebel, Hydrogen abstraction acetylene addition and Diels–Alder mechanisms of PAH formation: a detailed study using first principles calculations, J. Chem. Theory Comput. 1 (5) (2005) 908–924, doi:10.1021/ct0500491.
[24] J. Cioslowski, M. Schimeczek, P. Piskorz, D. Moncrieff, Thermal rearrangement of ethynylarenes to cyclopentafused polycyclic aromatic hydrocarbons: an electronic structure study, J. Am. Chem. Soc. 121 (15) (1999) 3773–3778, doi:10.1021/ja9836601.
[25] M. Frenklach, D.W. Clary, W.C. Gardiner, S.E. Stein, Detailed kinetic modeling of soot formation in shock-tube pyrolysis of acetylene, Symp. (Int.) Combust. 20 (1) (1985) 887–901, doi:10.1016/S0082-0784(85)80578-6.
[26] A. Ciajolo, A. Tregrossi, M. Mallardo, T. Faravelli, E. Ranzi, Experimental and kinetic modeling study of sooting atmospheric-pressure cyclohexane flame, Proc. Combust. Inst. 32 (1) (2009) 585–591, doi:10.1016/j.proci.2008.06.170.
[27] N. Hansen, J.A. Miller, T. Kasper, K. Kohse-Höinghaus, P.R. Westmoreland, J. Wang, T.A. Cool, Benzene formation in premixed fuel-rich 1,3-butadiene flames, Proc. Combust. Inst. 32 (1) (2009) 623–630, doi:10.1016/j.proci.2008.06.050.
[28] C. Marchal, J.-L. Delfau, C. Vovelle, G. Moréac, C. Mounaïm-Rousselle, F. Mauss, Modelling of aromatics and soot formation from large fuel molecules, Proc. Combust. Inst. 32 (1) (2009) 753–759, doi:10.1016/j.proci.2008.06.115.
[29] H. Wang, M. Frenklach, A detailed kinetic modeling study of aromatics formation in laminar premixed acetylene and ethylene flames, Combust. Flame 110 (1) (1997) 173–221, doi:10.1016/S0010-2180(97)00068-0.
[30] A. D'Anna, A. Violi, A. D'Alessio, Modeling the rich combustion of aliphatic hydrocarbons, Combust. Flame 121 (3) (2000) 418–429, doi:10.1016/S0010-2180(99)00163-7.
[31] A. D'Anna, A. Violi, A kinetic model for the formation of aromatic hydrocarbons in premixed laminar flames, Symp. (Int.) Combust. 27 (1) (1998) 425–433, doi:10.1016/S0082-0784(98)80431-1.
[32] P. Lindstedt, Modeling of the chemical complexities of flames, Symp. (Int.) Combust. 27 (1) (1998) 269–285, doi:10.1016/S0082-0784(98)80414-1.
[33] C. Saggese, S. Ferrario, J. Camacho, A. Cuoci, A. Frassoldati, E. Ranzi, H. Wang, T. Faravelli, Kinetic modeling of particle size distribution of soot in a premixed burner-stabilized stagnation ethylene flame, Combust. Flame 162 (9) (2015) 3356–3369, doi:10.1016/j.combustflame.2015.06.002.
[34] G. Blanquart, P. Pepiot-Desjardins, H. Pitsch, Chemical mechanism for high temperature combustion of engine relevant fuels with emphasis on soot precursors, Combust. Flame 156 (3) (2009) 588–607, doi:10.1016/j.combustflame.2008.12.007.
[35] G. Kukkadapu, S. Wagnon, W. Pitz, N. Hansen, Identification of the molecular-weight growth reaction network in counterflow flames of the C_3H_4 isomers allene and propyne, Proc. Combust. Inst. 38 (1) (2021) 1477–1485, doi:10.1016/j.proci.2020.07.130.
[36] N. Hansen, B. Yang, M. Braun-Unkhoff, A. Ramirez, G. Kukkadapu, Molecular-growth pathways in premixed flames of benzene and toluene doped with propyne, Combust. Flame (2022) 112075, doi:10.1016/j.combustflame.2022.112075.
[37] S. Dong, S.W. Wagnon, L. Pratali Maffei, G. Kukkadapu, A. Nobili, Q. Mao, M. Pelucchi, L. Cai, K. Zhang, M. Raju, T. Chatterjee, W.J. Pitz, T. Faravelli, H. Pitsch, P.K. Senecal, H.J. Curran, A new detailed kinetic model for surrogate fuels: C3MechV3.3, Appl. Energy Combust. Sci. 9 (2022) 100043, doi:10.1016/j.jaecs.2021.100043.
[38] M. Frenklach, A.M. Mebel, On the mechanism of soot nucleation, Phys. Chem. Chem. Phys. 22 (2020) 5314–5331, doi:10.1039/D0CP00116C.
[39] K. Bowal, J.W. Martin, A.J. Misquitta, M. Kraft, Ion-induced soot nucleation using a new potential for curved aromatics, Combust. Sci. Technol. 191 (5–6) (2019) 747–765, doi:10.1080/00102202.2019.1565496.
[40] M. Frenklach, N.W. Moriarty, N.J. Brown, Hydrogen migration in polyaromatic growth, Symp. (Int.) Combust. 27 (2) (1998) 1655–1661, doi:10.1016/S0082-0784(98)80004-0.
[41] M. Frenklach, On surface growth mechanism of soot particles, Symp. (Int.) Combust. 26 (2) (1996) 2285–2293, doi:10.1016/S0082-0784(96)80056-7.
[42] M. Frenklach, C.A. Schuetz, J. Ping, Migration mechanism of aromatic-edge growth, Proc. Combust. Inst. 30 (1) (2005) 1389–1396, doi:10.1016/j.proci.2004.07.048.
[43] R. Whitesides, A.C. Kollias, D. Domin, W.A. Lester, M. Frenklach, Graphene layer growth: collision of migrating five-member rings, Proc. Combust. Inst. 31 (1) (2007) 539–546, doi:10.1016/j.proci.2006.07.034.
[44] R. Whitesides, D. Domin, R. Salomón-Ferrer, W.A. Lester, M. Frenklach, Graphene layer growth chemistry: five- and six-member ring flip reaction, J. Phys. Chem. A 112 (10) (2008) 2125–2130, doi:10.1021/jp075785a.
[45] R. Whitesides, D. Domin, R. Salomón-Ferrer, W.A. Lester, M. Frenklach, Embedded-ring migration on graphene zigzag edge, Proc. Combust. Inst. 32 (1) (2009) 577–583, doi:10.1016/j.proci.2008.06.096.
[46] J.W. Martin, M. Salamanca, M. Kraft, Soot inception: carbonaceous nanoparticle formation in flames, Prog. Energy Combust. Sci. 88 (2022) 100956, doi:10.1016/j.pecs.2021.100956.
[47] K. Johansson, J. Lai, S. Skeen, D. Popolan-Vaida, K. Wilson, N. Hansen, A. Violi, H. Michelsen, Soot precursor formation and limitations of the stabilomer grid, Proc. Combust. Inst. 35 (2) (2015) 1819–1826, doi:10.1016/j.proci.2014.05.033.
[48] M. Commodo, K. Kaiser, G. De Falco, P. Minutolo, F. Schulz, A. D'Anna, L. Gross, On the early stages of soot formation: molecular structure elucidation by high-resolution atomic force microscopy, Combust. Flame 205 (2019) 154–164, doi:10.1016/j.combustflame.2019.03.042.
[49] F. Schulz, M. Commodo, K. Kaiser, G. De Falco, P. Minutolo, G. Meyer, A. D'Anna, L. Gross, Insights into incipient soot formation by atomic force microscopy, Proc. Combust. Inst. 37 (1) (2019) 885–892, doi:10.1016/j.proci.2018.06.100.
[50] D.S.N. Parker, R.I. Kaiser, B. Bandyopadhyay, O. Kostko, T.P. Troy, M. Ahmed, Unexpected chemistry from the reaction of naphthyl and acetylene at combustion-like temperatures, Angew. Chem. Int. Ed. 54 (18) (2015) 5421–5424, doi:10.1002/anie.201411987.
[51] L. Pascazio, J.W. Martin, A. Menon, D. Hou, X. You, M. Kraft, Aromatic pentalinked hydrocarbons in soot nanoparticle formation, Proc. Combust. Inst. 38 (1) (2021) 1525–1532, doi:10.1016/j.proci.2020.09.029.
[52] A. D'Anna, A. Violi, A. D'Alessio, A. Sarofim, A reaction pathway for nanoparticle formation in rich premixed flames, Combust. Flame 127 (1) (2001) 1995–2003, doi:10.1016/S0010-2180(01)00303-0.
[53] X. You, R. Whitesides, D. Zubarev, W.A. Lester, M. Frenklach, Bay-capping reactions: kinetics and influence on graphene-edge growth, Proc. Combust. Inst. 33 (1) (2011) 685–692, doi:10.1016/j.proci.2010.05.110.
[54] P. Liu, Z. Li, A. Bennett, H. Lin, S.M. Sarathy, W.L. Roberts, The site effect on PAHs formation in HACA-based mass growth process, Combust. Flame 199 (2019) 54–68, doi:10.1016/j.combustflame.2018.10.010.
[55] P. Liu, Z. Li, W.L. Roberts, Growth network of PAH with 5-membered ring: case study with acenaphthylene molecule, Combust. Flame 230 (2021) 111449, doi:10.1016/j.combustflame.2021.111449.
[56] T.-C. Chu, M.C. Smith, J. Yang, M. Liu, W.H. Green, Theoretical study on the HACA chemistry of naphthalenyl radicals and acetylene: the formation of $C_{12}H_8$, $C_{14}H_8$, and $C_{14}H_{10}$ species, Int. J. Chem. Kinet. 52 (11) (2020) 752–768, doi:10.1002/kin.21397.
[57] A.S. Savchenkova, I.V. Chechet, S.G. Matveev, M. Frenklach, A.M. Mebel, Formation of phenanthrenyl radicals via the reaction of acenaphthyl with acetylene, Proc. Combust. Inst. 38 (1) (2021) 1441–1448, doi:10.1016/j.proci.2020.06.347.
[58] A.D. Abid, J. Camacho, D.A. Sheen, H. Wang, Quantitative measurement of soot particle size distribution in premixed flames – the burner-stabilized stagnation flame approach, Combust. Flame 156 (10) (2009) 1862–1870, doi:10.1016/j.combustflame.2009.05.010.
[59] S. Park, Y. Wang, S.H. Chung, S.M. Sarathy, Compositional effects on PAH and soot formation in counterflow diffusion flames of gasoline surrogate fuels, Combust. Flame 178 (2017) 46–60, doi:10.1016/j.combustflame.2017.01.001.

[60] C. Shao, H. Wang, N. Atef, Z. Wang, B. Chen, M. Almalki, Y. Zhang, C. Cao, J. Yang, S.M. Sarathy, Polycyclic aromatic hydrocarbons in pyrolysis of gasoline surrogates (*n*-heptane/iso-octane/toluene), Proc. Combust. Inst. 37 (1) (2019) 993–1001, doi:10.1016/j.proci.2018.06.087.
[61] G. Kukkadapu, D. Kang, S.W. Wagnon, K. Zhang, M. Mehl, M. Monge-Palacios, H. Wang, S.S. Goldsborough, C.K. Westbrook, W.J. Pitz, Kinetic modeling study of surrogate components for gasoline, jet and diesel fuels: C7–C11 methylated aromatics, Proc. Combust. Inst. 37 (1) (2019) 521–529, doi:10.1016/j.proci.2018.08.016.
[62] L. Cai, A. Ramalingam, H. Minwegen, K. Alexander Heufer, H. Pitsch, Impact of exhaust gas recirculation on ignition delay times of gasoline fuel: an experimental and modeling study, Proc. Combust. Inst. 37 (1) (2019) 639–647, doi:10.1016/j.proci.2018.05.032.
[63] K. Narayanaswamy, G. Blanquart, H. Pitsch, A consistent chemical mechanism for oxidation of substituted aromatic species, Combust. Flame 157 (10) (2010) 1879–1898, doi:10.1016/j.combustflame.2010.07.009.
[64] L. Cai, H. Pitsch, Optimized chemical mechanism for combustion of gasoline surrogate fuels, Combust. Flame 162 (5) (2015) 1623–1637, doi:10.1016/j.combustflame.2014.11.018.
[65] N. Hansen, J.A. Miller, S.J. Klippenstein, P.R. Westmoreland, K. Kohse-Höinghaus, Exploring formation pathways of aromatic compounds in laboratory-based model flames of aliphatic fuels, Combust. Explos. Shock Waves 48 (5) (2012) 508–515, doi:10.1134/S0010508212050024.
[66] M. Frenklach, R.I. Singh, A.M. Mebel, On the low-temperature limit of HACA, Proc. Combust. Inst. 37 (1) (2019) 969–976, doi:10.1016/j.proci.2018.05.068.
[67] Y. Wu, S. Panigrahy, A.B. Sahu, C. Bariki, J. Beeckmann, J. Liang, A.A. Mohamed, S. Dong, C. Tang, H. Pitsch, Z. Huang, H.J. Curran, Understanding the antagonistic effect of methanol as a component in surrogate fuel models: a case study of methanol/*n*-heptane mixtures, Combust. Flame 226 (2021) 229–242, doi:10.1016/j.combustflame.2020.12.006.
[68] A. Ramalingam, S. Panigrahy, Y. Fenard, H. Curran, K.A. Heufer, A chemical kinetic perspective on the low-temperature oxidation of propane/propene mixtures through experiments and kinetic analyses, Combust. Flame 223 (2021) 361–375, doi:10.1016/j.combustflame.2020.10.020.
[69] M. Baigmohammadi, V. Patel, S. Nagaraja, A. Ramalingam, S. Martinez, S. Panigrahy, A.A.E.-S. Mohamed, K.P. Somers, U. Burke, K.A. Heufer, A. Pekalski, H.J. Curran, Comprehensive experimental and simulation study of the ignition delay time characteristics of binary blended methane, ethane, and ethylene over a wide range of temperature, pressure, equivalence ratio, and dilution, Energy Fuels 34 (7) (2020) 8808–8823, doi:10.1021/acs.energyfuels.0c00960.
[70] S.S. Nagaraja, J. Liang, S. Dong, S. Panigrahy, A. Sahu, G. Kukkadapu, S.W. Wagnon, W.J. Pitz, H.J. Curran, A hierarchical single-pulse shock tube pyrolysis study of C_2–C_6 1-alkenes, Combust. Flame 219 (2020) 456–466, doi:10.1016/j.combustflame.2020.06.021.
[71] N. Lokachari, S. Panigrahy, G. Kukkadapu, G. Kim, S.S. Vasu, W.J. Pitz, H.J. Curran, The influence of iso-butene kinetics on the reactivity of di-isobutylene and iso-octane, Combust. Flame 222 (2020) 186–195, doi:10.1016/j.combustflame.2020.08.007.
[72] S. Panigrahy, J. Liang, S.S. Nagaraja, Z. Zuo, G. Kim, S. Dong, G. Kukkadapu, W.J. Pitz, S.S. Vasu, H.J. Curran, A comprehensive experimental and improved kinetic modeling study on the pyrolysis and oxidation of propyne, Proc. Combust. Inst. 38 (1) (2021) 479–488, doi:10.1016/j.proci.2020.06.320.
[73] A.A. El-Sabor Mohamed, S. Panigrahy, A.B. Sahu, G. Bourque, H.J. Curran, An experimental and kinetic modeling study of the auto-ignition of natural gas blends containing C_1–C_7 alkanes, Proc. Combust. Inst. 38 (1) (2021) 365–373, doi:10.1016/j.proci.2020.06.015.
[74] S.S. Nagaraja, J. Power, G. Kukkadapu, S. Dong, S.W. Wagnon, W.J. Pitz, H.J. Curran, A single pulse shock tube study of pentene isomer pyrolysis, Proc. Combust. Inst. 38 (1) (2021) 881–889, doi:10.1016/j.proci.2020.06.069.
[75] S. Dong, K. Zhang, E.M. Ninnemann, A. Najjar, G. Kukkadapu, J. Baker, F. Arafin, Z. Wang, W.J. Pitz, S.S. Vasu, S.M. Sarathy, P.K. Senecal, H.J. Curran, A comprehensive experimental and kinetic modeling study of 1- and 2-pentene, Combust. Flame 223 (2021) 166–180, doi:10.1016/j.combustflame.2020.09.012.
[76] S.S. Nagaraja, G. Kukkadapu, S. Panigrahy, J. Liang, H. Lu, W.J. Pitz, H.J. Curran, A pyrolysis study of allylic hydrocarbon fuels, Int. J. Chem. Kinet. 52 (12) (2020) 964–978, doi:10.1002/kin.21414.
[77] S. Dong, K. Zhang, P.K. Senecal, G. Kukkadapu, S.W. Wagnon, S. Barrett, N. Lokachari, S. Panigaphy, W.J. Pitz, H.J. Curran, A comparative reactivity study of 1-alkene fuels from ethylene to 1-heptene, Proc. Combust. Inst. 38 (1) (2021) 611–619, doi:10.1016/j.proci.2020.07.053.
[78] W.K. Metcalfe, S.M. Burke, S.S. Ahmed, H.J. Curran, A hierarchical and comparative kinetic modeling study of C_1–C_2 hydrocarbon and oxygenated fuels, Int. J. Chem. Kinet. 45 (10) (2013) 638–675, doi:10.1002/kin.20802.
[79] S.M. Burke, U. Burke, R. Mc Donagh, O. Mathieu, I. Osorio, C. Keesee, A. Morones, E.L. Petersen, W. Wang, T.A. DeVerter, M.A. Oehlschlaeger, B. Rhodes, R.K. Hanson, D.F. Davidson, B.W. Weber, C.-J. Sung, J. Santner, Y. Ju, F.M. Haas, F.L. Dryer, E.N. Volkov, E.J. Nilsson, A.A. Konnov, M. Alrefae, F. Khaled, A. Farooq, P. Dirrenberger, P.-A. Glaude, F. Battin-Leclerc, H.J. Curran, An experimental and modeling study of propene oxidation. Part 2: ignition delay time and flame speed measurements, Combust. Flame 162 (2) (2015) 296–314, doi:10.1016/j.combustflame.2014.07.032.
[80] S.M. Burke, W. Metcalfe, O. Herbinet, F. Battin-Leclerc, F.M. Haas, J. Santner, F.L. Dryer, H.J. Curran, An experimental and modeling study of propene oxidation. Part 1: speciation measurements in jet-stirred and flow reactors, Combust. Flame 161 (11) (2014) 2765–2784, doi:10.1016/j.combustflame.2014.05.010.
[81] A. Kéromnès, W.K. Metcalfe, K.A. Heufer, N. Donohoe, A.K. Das, C.-J. Sung, J. Herzler, C. Naumann, P. Griebel, O. Mathieu, M.C. Krejci, E.L. Petersen, W.J. Pitz, H.J. Curran, An experimental and detailed chemical kinetic modeling study of hydrogen and syngas mixture oxidation at elevated pressures, Combust. Flame 160 (6) (2013) 995–1011, doi:10.1016/j.combustflame.2013.01.001.
[82] C.-W. Zhou, Y. Li, U. Burke, C. Banyon, K.P. Somers, S. Ding, S. Khan, J.W. Hargis, T. Sikes, O. Mathieu, E.L. Petersen, M. AlAbbad, A. Farooq, Y. Pan, Y. Zhang, Z. Huang, J. Lopez, Z. Loparo, S.S. Vasu, H.J. Curran, An experimental and chemical kinetic modeling study of 1,3-butadiene combustion: ignition delay time and laminar flame speed measurements, Combust. Flame 197 (2018) 423–438, doi:10.1016/j.combustflame.2018.08.006.
[83] C.W. Gao, J.W. Allen, W.H. Green, R.H. West, Reaction mechanism generator: automatic construction of chemical kinetic mechanisms, Comput. Phys. Commun. 203 (2016) 212–225, doi:10.1016/j.cpc.2016.02.013.
[84] S.R. Heller, A. McNaught, I. Pletnev, S. Stein, D. Tchekhovskoi, InChI, the IUPAC international chemical identifier, J. Cheminformatics 7 (1) (2015) 1–34.
[85] D. Weininger, SMILES, a chemical language and information system. 1. Introduction to methodology and encoding rules, J. Chem. Inf. Comput. Sci. 28 (1) (1988) 31–36, doi:10.1021/ci00057a005.
[86] G. Landrum, RDKit: open-source cheminformatics software(2021).
[87] M. Frenklack, W. Gardiner, S. Stein, D. Clary, T. Yuan, Mechanism of soot formation in acetylene-oxygen mixtures, Combust. Sci. Technol. 50 (1–3) (1986) 79–115, doi:10.1080/00102208608923927.
[88] J.A. Miller, J.P. Senosiain, S.J. Klippenstein, Y. Georgievskii, Reactions over multiple, interconnected potential wells: unimolecular and bimolecular reactions on a C_3H_5 potential, J. Phys. Chem. A 112 (39) (2008) 9429–9438, doi:10.1021/jp804510k.
[89] J.A. Miller, S.J. Klippenstein, From the multiple-well master equation to phenomenological rate coefficients: reactions on a C_3H_4 potential energy surface, J. Phys. Chem. A 107 (15) (2003) 2680–2692, doi:10.1021/jp0221082.
[90] S.J. Klippenstein, J.A. Miller, A.W. Jasper, Kinetics of propargyl radical dissociation, J. Phys. Chem. A 119 (28) (2015) 7780–7791, doi:10.1021/acs.jpca.5b01127.
[91] L. Ye, Y. Georgievskii, S.J. Klippenstein, Pressure-dependent branching in the reaction of $^1CH_2$ with C_2H_4 and other reactions on the C_3H_6 potential energy surface, Proc. Combust. Inst. 35 (1) (2015) 223–230, doi:10.1016/j.proci.2014.05.097.
[92] J.A. Miller, S.J. Klippenstein, Dissociation of propyl radicals and other reactions on a C_3H_7 potential, J. Phys. Chem. A 117 (13) (2013) 2718–2727, doi:10.1021/jp312712p.
[93] R. Sivaramakrishnan, M.-C. Su, J.V. Michael, S.J. Klippenstein, L.B. Harding, B. Ruscic, Shock tube and theoretical studies on the thermal decomposition of propane: evidence for a roaming radical channel, J. Phys. Chem. A 115 (15) (2011) 3366–3379, doi:10.1021/jp2006205.
[94] J. Zádor, J.A. Miller, Adventures on the C_3H_5O potential energy surface: OH + propyne, OH + allene and related reactions, Proc. Combust. Inst. 35 (1) (2015) 181–188, doi:10.1016/j.proci.2014.05.103.
[95] I. Gimondi, C. Cavallotti, G. Vanuzzo, N. Balucani, P. Casavecchia, Reaction dynamics of $O(^3P)$ + propyne: II. Primary products, branching ratios, and role of intersystem crossing from ab initio coupled triplet/singlet potential energy surfaces and statistical calculations, J. Phys. Chem. A 120 (27) (2016) 4619–4633, doi:10.1021/acs.jpca.6b01564.
[96] G. Vanuzzo, N. Balucani, F. Leonori, D. Stranges, S. Falcinelli, A. Bergeat, P. Casavecchia, I. Gimondi, C. Cavallotti, Isomer-specific chemistry in the propyne and allene reactions with oxygen atoms: CH_3CH + CO versus CH_2CH_2 + CO products, J. Phys. Chem. Lett. 7 (6) (2016) 1010–1015, doi:10.1021/acs.jpclett.6b00262.
[97] A. Fridlyand, P.T. Lynch, R.S. Tranter, K. Brezinsky, Single pulse shock tube study of allyl radical recombination, J. Phys. Chem. A 117 (23) (2013) 4762–4776, doi:10.1021/jp402391n.
[98] J. Zádor, A.W. Jasper, J.A. Miller, The reaction between propene and hydroxyl, Phys. Chem. Chem. Phys. 11 (2009) 11040–11053, doi:10.1039/B915707G.
[99] Y. Bedjanian, J. Morin, Reaction of $O(^3P)$ with C_3H_6: yield of the reaction products as a function of temperature, J. Phys. Chem. A 121 (8) (2017) 1553–1562, doi:10.1021/acs.jpca.6b12739.
[100] X. Chen, C.F. Goldsmith, A theoretical and computational analysis of the methyl-vinyl + O_2 reaction and its effects on propene combustion, J. Phys. Chem. A 121 (48) (2017) 9173–9184, doi:10.1021/acs.jpca.7b07594.
[101] C.F. Goldsmith, L.B. Harding, Y. Georgievskii, J.A. Miller, S.J. Klippenstein, Temperature and pressure-dependent rate coefficients for the reaction of vinyl radical with molecular oxygen, J. Phys. Chem. A 119 (28) (2015) 7766–7779, doi:10.1021/acs.jpca.5b01088.
[102] J. Wullenkord, I. Graf, M. Baroncelli, D. Felsmann, L. Cai, H. Pitsch, K. Kohse-Höinghaus, Laminar premixed and non-premixed flame investigation on the influence of dimethyl ether addition on *n*-heptane combustion, Combust. Flame 212 (2020) 323–336, doi:10.1016/j.combustflame.2019.11.012.
[103] F. Carbone, A. Gomez, The structure of toluene-doped counterflow gaseous diffusion flames, Combust. Flame 159 (10) (2012) 3040–3055, doi:10.1016/j.combustflame.2012.05.003.
[104] M. Baroncelli, D. Felsmann, N. Hansen, H. Pitsch, Investigating the effect of oxy-fuel combustion and light coal volatiles interaction: a mass spectrometric study, Combust. Flame 204 (2019) 320–330, doi:10.1016/j.combustflame.2019.03.017.

[105] L. Figura, A. Gomez, Structure of incipiently sooting ethylene-nitrogen counterflow diffusion flames at high pressures, Combust. Flame 161 (6) (2014) 1587–1603, doi:10.1016/j.combustflame.2013.11.023.
[106] D.S.N. Parker, F. Zhang, Y.S. Kim, R.I. Kaiser, A. Landera, V.V. Kislov, A.M. Mebel, A.G.G.M. Tielens, Low temperature formation of naphthalene and its role in the synthesis of PAHs (polycyclic aromatic hydrocarbons) in the interstellar medium, Proc. Natl. Acad. Sci. 109 (1) (2012) 53–58, doi:10.1073/pnas.1113827108.
[107] L. Monluc, A.A. Nikolayev, I.A. Medvedkov, V.N. Azyazov, A.N. Morozov, A.M. Mebel, The reaction of *o*-benzyne with vinylacetylene: an unexplored way to produce naphthalene, ChemPhysChem 23 (2) (2022) e202100758, doi:10.1002/cphc.202100758.
[108] A.M. Mebel, A. Landera, R.I. Kaiser, Formation mechanisms of naphthalene and indene: from the interstellar medium to combustion flames, J. Phys. Chem. A 121 (5) (2017) 901–926, doi:10.1021/acs.jpca.6b09735.
[109] C. Shao, G. Kukkadapu, S.W. Wagnon, W.J. Pitz, S.M. Sarathy, PAH formation from jet stirred reactor pyrolysis of gasoline surrogates, Combust. Flame 219 (2020) 312–326, doi:10.1016/j.combustflame.2020.06.001.
[110] D. Polino, C. Cavallotti, Fulvenallene decomposition kinetics, J. Phys. Chem. A 115 (37) (2011) 10281–10289, doi:10.1021/jp202756s.
[111] M. Derudi, D. Polino, C. Cavallotti, Toluene and benzyl decomposition mechanisms: elementary reactions and kinetic simulations, Phys. Chem. Chem. Phys. 13 (2011) 21308–21318, doi:10.1039/C1CP22601K.
[112] G. da Silva, J.W. Bozzelli, The C_7H_5 fulvenallenyl radical as a combustion intermediate: potential new pathways to two- and three-ring PAHs, J. Phys. Chem. A 113 (44) (2009) 12045–12048, doi:10.1021/jp907230b.
[113] H. Jin, L. Xing, J. Yang, Z. Zhou, F. Qi, A. Farooq, Continuous butadiyne addition to propargyl: aradical-efficient pathway for polycyclic aromatic hydrocarbons, J. Phys. Chem. Lett. 12 (33) (2021) 8109–8114, doi:10.1021/acs.jpclett.1c02062.
[114] J. Bai, C. Cavallotti, C.-W. Zhou, Theoretical kinetics analysis for OH radical addition to 1,3-butadiene and application to model prediction, Combust. Flame 221 (2020) 228–240, doi:10.1016/j.combustflame.2020.07.036.
[115] S.J. Klippenstein, J.A. Miller, The addition of hydrogen atoms to diacetylene and the heats of formation of *i*-C_4H_3 and *n*-C_4H_3, J. Phys. Chem. A 109 (19) (2005) 4285–4295, doi:10.1021/jp058017x.
[116] J. Zádor, M.D. Fellows, J.A. Miller, Initiation reactions in acetylene pyrolysis, J. Phys. Chem. A 121 (22) (2017) 4203–4217, doi:10.1021/acs.jpca.7b03040.
[117] J.M. Ribeiro, A.M. Mebel, Reaction mechanism and product branching ratios of the CH + C_3H_4 reactions: a theoretical study, Phys. Chem. Chem. Phys. 19 (2017) 14543–14554, doi:10.1039/C7CP01873H.
[118] K.S. Shin, J.V. Michael, Rate constants (296–1700 K) for the reactions $C_2H + C_2H_2 \rightarrow C_4H_2 + H$ and $C_2D + C_2D_2 \rightarrow C_4D_2 + D$, J. Phys. Chem. 95 (15) (1991) 5864–5869.
[119] J.O.P. Pedersen, B.J. Opansky, S.R. Leone, Laboratory studies of low-temperature reactions of ethynyl with acetylene and implications for atmospheric models of Titan, J. Phys. Chem. 97 (26) (1993) 6822–6829.
[120] P.T. Lynch, C.J. Annesley, R.S. Tranter, Dissociation of *ortho*-benzyne radicals in the high temperature fall-off regime, Proc. Combust. Inst. 35 (1) (2015) 145–152, doi:10.1016/j.proci.2014.05.049.
[121] J.P. Senosiain, S.J. Klippenstein, J.A. Miller, Oxidation pathways in the reaction of diacetylene with OH radicals, Proc. Combust. Inst. 31 (1) (2007) 185–192, doi:10.1016/j.proci.2006.08.084.
[122] Y. Hidaka, Y. Henmi, T. Ohonishi, T. Okuno, T. Koike, Shock-tube and modeling study of diacetylene pyrolysis and oxidation, Combust. Flame 130 (1) (2002) 62–82, doi:10.1016/S0010-2180(02)00365-6.
[123] R.J. Cvetanović, Evaluated chemical kinetic data for the reactions of atomic oxygen $O(^3P)$ with unsaturated hydrocarbons, J. Phys. Chem. Ref. Data 16 (2) (1987) 261–326, doi:10.1063/1.555783.
[124] S.S. Vasu, J. Zádor, D.F. Davidson, R.K. Hanson, D.M. Golden, J.A. Miller, High-temperature measurements and a theoretical study of the reaction of OH with 1,3-butadiene, J. Phys. Chem. A 114 (32) (2010) 8312–8318, doi:10.1021/jp104880u.
[125] Y. Li, S.J. Klippenstein, C.-W. Zhou, H.J. Curran, Theoretical kinetics analysis for Ḣ atom addition to 1,3-butadiene and related reactions on the C_4H_7 potential energy surface, J. Phys. Chem. A 121 (40) (2017) 7433–7445, doi:10.1021/acs.jpca.7b05996.
[126] J.P. Senosiain, J.A. Miller, The reaction of *n*- and *i*-C_4H_5 radicals with acetylene, J. Phys. Chem. A 111 (19) (2007) 3740–3747, doi:10.1021/jp0675126.
[127] J.P.A. Lockhart, C.F. Goldsmith, J.B. Randazzo, B. Ruscic, R.S. Tranter, An experimental and theoretical study of the thermal decomposition of C_4H_6 isomers, J. Phys. Chem. A 121 (20) (2017) 3827–3850, doi:10.1021/acs.jpca.7b01186.
[128] L.K. Rutz, G. da Silva, J.W. Bozzelli, H. Bockhorn, Reaction of the *i*-C_4H_5 (CH_2CCHCH_2) radical with O_2, J. Phys. Chem. A 115 (6) (2011) 1018–1026, doi:10.1021/jp1072439.
[129] C.-Y. Lin, M.C. Lin, Unimolecular decomposition of the phenoxy radical in shock waves, Int. J. Chem. Kinet. 17 (10) (1985) 1025–1028, doi:10.1002/kin.550171002.
[130] X. Zhong, J.W. Bozzelli, Thermochemical and kinetic analysis on the addition reactions of H, O, OH, and HO_2 with 1,3-cyclopentadiene, Int. J. Chem. Kinet. 29 (12) (1997) 893–913, doi:10.1002/(SICI)1097-4601(1997)29:12<893::AID-KIN2>3.0.CO;2-H.
[131] X. Zhong, J.W. Bozzelli, Thermochemical and kinetic analysis of the H, OH, HO_2, O, and O_2 association reactions with cyclopentadienyl radical, J. Phys. Chem. A 102 (20) (1998) 3537–3555, doi:10.1021/jp9804446.
[132] A.N. Morozov, I.A. Medvedkov, V.N. Azyazov, A.M. Mebel, Theoretical study of the phenoxy radical recombination with the $O(^3P)$ atom, phenyl plus molecular oxygen revisited, J. Phys. Chem. A 125 (18) (2021) 3965–3977, doi:10.1021/acs.jpca.1c01545.
[133] M. Baroncelli, Q. Mao, S. Galle, N. Hansen, H. Pitsch, Role of ring-enlargement reactions in the formation of aromatic hydrocarbons, Phys. Chem. Chem. Phys. 22 (2020) 4699–4714, doi:10.1039/C9CP05854K.
[134] K.O. Johansson, M.P. Head-Gordon, P.E. Schrader, K.R. Wilson, H.A. Michelsen, Resonance-stabilized hydrocarbon-radical chain reactions may explain soot inception and growth, Science 361 (6406) (2018) 997–1000, doi:10.1126/science.aat3417.
[135] A.E. Long, S.S. Merchant, A.G. Vandeputte, H.-H. Carstensen, A.J. Vervust, G.B. Marin, K.M. Van Geem, W.H. Green, Pressure dependent kinetic analysis of pathways to naphthalene from cyclopentadienyl recombination, Combust. Flame 187 (2018) 247–256, doi:10.1016/j.combustflame.2017.09.008.
[136] S. Sharma, W.H. Green, Computed rate coefficients and product yields for c-C_5H_5 + $CH_3 \rightarrow$ Products, J. Phys. Chem. A 113 (31) (2009) 8871–8882, doi:10.1021/jp900679t.
[137] Q. Mao, C. Huang, M. Baroncelli, L. Shen, L. Cai, K. Leonhard, H. Pitsch, Unimolecular reactions of the resonance-stabilized cyclopentadienyl radicals and their role in the polycyclic aromatic hydrocarbon formation, Proc. Combust. Inst. 38 (1) (2021) 729–737, doi:10.1016/j.proci.2020.08.009.
[138] Q. Mao, L. Cai, R. Langer, H. Pitsch, The role of resonance-stabilized radical chain reactions in polycyclic aromatic hydrocarbon growth: theoretical calculation and kinetic modeling, Proc. Combust. Inst. 38 (1) (2021) 1459–1466, doi:10.1016/j.proci.2020.07.117.
[139] R. Robinson, R. Lindstedt, On the chemical kinetics of cyclopentadiene oxidation, Combust. Flame 158 (4) (2011) 666–686, doi:10.1016/j.combustflame.2010.12.001.
[140] A.D. Oleinikov, V.N. Azyazov, A.M. Mebel, Oxidation of cyclopentadienyl radical with molecular oxygen: a theoretical study, Combust. Flame 191 (2018) 309–319, doi:10.1016/j.combustflame.2018.01.010.
[141] G. Galimova, V. Azyazov, A. Mebel, Reaction mechanism, rate constants, and product yields for the oxidation of cyclopentadienyl and embedded five-member ring radicals with hydroxyl, Combust. Flame 187 (2018) 147–164, doi:10.1016/j.combustflame.2017.09.005.
[142] A. Ghildina, A. Oleinikov, V. Azyazov, A. Mebel, Reaction mechanism, rate constants, and product yields for unimolecular and H-assisted decomposition of 2,4-cyclopentadienone and oxidation of cyclopentadienyl with atomic oxygen, Combust. Flame 183 (2017) 181–193, doi:10.1016/j.combustflame.2017.05.015.
[143] A. Lamprecht, B. Atakan, K. Kohse-Höinghaus, Fuel-rich flame chemistry in low-pressure cyclopentene flames, Proc. Combust. Inst. 28 (2) (2000) 1817–1824, doi:10.1016/S0082-0784(00)80584-6.
[144] N. Hansen, T. Kasper, S.J. Klippenstein, P.R. Westmoreland, M.E. Law, C.A. Taatjes, K. Kohse-Höinghaus, J. Wang, T.A. Cool, Initial steps of aromatic ring formation in a laminar premixed fuel-rich cyclopentene flame, J. Phys. Chem. A 111 (19) (2007) 4081–4092, doi:10.1021/jp0683317.
[145] A.M. Mebel, Y. Georgievskii, A.W. Jasper, S.J. Klippenstein, Pressure-dependent rate constants for PAH growth: formation of indene and its conversion to naphthalene, Faraday Discuss. 195 (2016) 637–670, doi:10.1039/C6FD00111D.
[146] A.M. Mebel, Y. Georgievskii, A.W. Jasper, S.J. Klippenstein, Temperature- and pressure-dependent rate coefficients for the HACA pathways from benzene to naphthalene, Proc. Combust. Inst. 36 (1) (2017) 919–926, doi:10.1016/j.proci.2016.07.013.
[147] L.P. Maffei, M. Pelucchi, R.D. Büttgen, K.A. Heufer, T. Faravelli, C. Cavallotti, Rate constants for the H-abstraction reactions from mono-aromatic hydrocarbons by Ḣ, $\dot{C}H_3$, ȮH and O_2: a systematic theoretical investigation (Unpublished results).
[148] C. Saggese, A. Frassoldati, A. Cuoci, T. Faravelli, E. Ranzi, A wide range kinetic modeling study of pyrolysis and oxidation of benzene, Combust. Flame 160 (7) (2013) 1168–1190, doi:10.1016/j.combustflame.2013.02.013.
[149] C. Cavallotti, C. De Falco, L. Pratali Maffei, A. Caracciolo, G. Vanuzzo, N. Balucani, P. Casavecchia, Theoretical study of the extent of intersystem crossing in the $O(^3P)$ + C_6H_6 reaction with experimental validation, J. Phys. Chem. Lett. 11 (22) (2020) 9621–9628, doi:10.1021/acs.jpclett.0c02866.
[150] L. Pratali Maffei, M. Pelucchi, T. Faravelli, C. Cavallotti, Theoretical study of sensitive reactions in phenol decomposition, React. Chem. Eng. 5 (2020) 452–472, doi:10.1039/C9RE00418A.
[151] L. Pratali Maffei, T. Faravelli, C. Cavallotti, M. Pelucchi, Electronic structure-based rate rules for Ḣ ipso addition–elimination reactions on mono-aromatic hydrocarbons with single and double OH/CH_3/OCH_3/CHO/C_2H_5 substituents: asystematic theoretical investigation, Phys. Chem. Chem. Phys. 22 (2020) 20368–20387, doi:10.1039/D0CP03099F.
[152] M. Pelucchi, C. Cavallotti, T. Faravelli, S.J. Klippenstein, H-abstraction reactions by OH, HO_2, O, O_2 and benzyl radical addition to O_2 and their implications for kinetic modelling of toluene oxidation, Phys. Chem. Chem. Phys. 20 (2018) 10607–10627, doi:10.1039/C7CP07779C.
[153] S.-H. Li, J.-J. Guo, R. Li, F. Wang, X.-Y. Li, Theoretical prediction of rate constants for hydrogen abstraction by OH, H, O, CH_3, and HO_2 radicals from toluene, J. Phys. Chem. A 120 (20) (2016) 3424–3432, doi:10.1021/acs.jpca.6b03049.
[154] G. da Silva, C.-C. Chen, J.W. Bozzelli, Toluene combustion: reaction paths, thermochemical properties, and kinetic analysis for the methylphenyl radical + O_2 reaction, J. Phys. Chem. A 111 (35) (2007) 8663–8676, doi:10.1021/jp068640x.
[155] G. da Silva, J.W. Bozzelli, Kinetic modeling of the benzyl + HO_2 reaction, Proc. Combust. Inst. 32 (1) (2009) 287–294, doi:10.1016/j.proci.2008.05.040.

[156] C.A. Taatjes, D.L. Osborn, T.M. Selby, G. Meloni, A.J. Trevitt, E. Epifanovsky, A.I. Krylov, B. Sirjean, E. Dames, H. Wang, Products of the benzene + O(^{3}P) reaction, J. Phys. Chem. A 114 (9) (2010) 3355–3370, doi:10.1021/jp9114145.
[157] A. Matsugi, A. Miyoshi, Computational study on the recombination reaction between benzyl and propargyl radicals, Int. J. Chem. Kinet. 44 (3) (2012) 206–218, doi:10.1002/kin.20625.
[158] E. Dames, H. Wang, Isomerization kinetics of benzylic and methylphenyl type radicals in single-ring aromatics, Proc. Combust. Inst. 34 (1) (2013) 307–314, doi:10.1016/j.proci.2012.05.014.
[159] C. Cavallotti, M. Derudi, R. Rota, On the mechanism of decomposition of the benzyl radical, Proc. Combust. Inst. 32 (1) (2009) 115–121, doi:10.1016/j.proci.2008.06.203.
[160] W. Yuan, Y. Li, G. Pengloan, C. Togbé, P. Dagaut, F. Qi, A comprehensive experimental and kinetic modeling study of ethylbenzene combustion, Combust. Flame 166 (2016) 255–265, doi:10.1016/j.combustflame.2016.01.026.
[161] A. Matsugi, A. Miyoshi, Modeling of two- and three-ring aromatics formation in the pyrolysis of toluene, Proc. Combust. Inst. 34 (1) (2013) 269–277, doi:10.1016/j.proci.2012.06.032.
[162] T.-C. Chu, Z.J. Buras, B. Eyob, M.C. Smith, M. Liu, W.H. Green, Direct kinetics and product measurement of phenyl radical + ethylene, J. Phys. Chem. A 124 (12) (2020) 2352–2365, doi:10.1021/acs.jpca.9b11543.
[163] T. Litzinger, K. Brezinsky, I. Glassman, The oxidation of ethylbenzene near 1060 K, Combust. Flame 63 (1) (1986) 251–267, doi:10.1016/0010-2180(86)90125-2.
[164] T. Sikes, C. Banyon, R.A. Schwind, P.T. Lynch, A. Comandini, R. Sivaramakrishnan, R.S. Tranter, Initiation reactions in the high temperature decomposition of styrene, Phys. Chem. Chem. Phys. 23 (2021) 18432–18448, doi:10.1039/D1CP02437J.
[165] M. Grela, V. Amorebieta, A. Colussi, Pyrolysis of styrene: kinetics and mechanism of the equilibrium styrene ⇌ benzene + acetylene, J. Phys. Chem. 96 (24) (1992) 9861–9865.
[166] S. Sharma, M.R. Harper, W.H. Green, Modeling of 1,3-hexadiene, 2,4-hexadiene and 1,4-hexadiene-doped methane flames: flame modeling, benzene and styrene formation, Combust. Flame 157 (7) (2010) 1331–1345, doi:10.1016/j.combustflame.2010.02.012.
[167] W. Yuan, Y. Li, P. Dagaut, J. Yang, F. Qi, Experimental and kinetic modeling study of styrene combustion, Combust. Flame 162 (5) (2015) 1868–1883, doi:10.1016/j.combustflame.2014.12.008.
[168] X. Li, A.W. Jasper, J. Zádor, J.A. Miller, S.J. Klippenstein, Theoretical kinetics of O + C_2H_4, Proc. Combust. Inst. 36 (1) (2017) 219–227, doi:10.1016/j.proci.2016.06.053.
[169] A.R. Ghildina, D.P. Porfiriev, V.N. Azyazov, A.M. Mebel, The mechanism and rate constants for oxidation of indenyl radical C_9H_7 with molecular oxygen O_2: a theoretical study, Phys. Chem. Chem. Phys. 21 (2019) 8915–8924, doi:10.1039/C9CP01122F.
[170] A.R. Ghildina, D.P. Porfiriev, V.N. Azyazov, A.M. Mebel, Scission of the five-membered ring in 1-*H*-Inden-1-one C_9H_6O and indenyl C_9H_7 in the reactions with H and O atoms, J. Phys. Chem. A 123 (27) (2019) 5741–5752, doi:10.1021/acs.jpca.9b04578.
[171] N. Hansen, M. Schenk, K. Moshammer, K. Kohse-Höinghaus, Investigating repetitive reaction pathways for the formation of polycyclic aromatic hydrocarbons in combustion processes, Combust. Flame 180 (2017) 250–261, doi:10.1016/j.combustflame.2016.09.013.
[172] J.A. Miller, S.J. Klippenstein, The recombination of propargyl radicals and other reactions on a C_6H_6 potential, J. Phys. Chem. A 107 (39) (2003) 7783–7799, doi:10.1021/jp030375h.
[173] J.A. Miller, S.J. Klippenstein, Y. Georgievskii, L.B. Harding, W.D. Allen, A.C. Simmonett, Reactions between resonance-stabilized radicals: propargyl + allyl, J. Phys. Chem. A 114 (14) (2010) 4881–4890, doi:10.1021/jp910604b.
[174] A.W. Jasper, N. Hansen, Hydrogen-assisted isomerizations of fulvene to benzene and of larger cyclic aromatic hydrocarbons, Proc. Combust. Inst. 34 (1) (2013) 279–287, doi:10.1016/j.proci.2012.06.165.
[175] A.N. Morozov, A.M. Mebel, Theoretical study of the reaction mechanism and kinetics of the phenyl + propargyl association, Phys. Chem. Chem. Phys. 22 (2020) 6868–6880, doi:10.1039/D0CP00306A.
[176] C. Cavallotti, D. Polino, A. Frassoldati, E. Ranzi, Analysis of some reaction pathways active during cyclopentadiene pyrolysis, J. Phys. Chem. A 116 (13) (2012) 3313–3324, doi:10.1021/jp212151p.
[177] S. Fascella, C. Cavallotti, R. Rota, S. Carrà, Quantum chemistry investigation of key reactions involved in the formation of naphthalene and indene, J. Phys. Chem. A 108 (17) (2004) 3829–3843, doi:10.1021/jp037518k.
[178] S.P. Sundar, S. Al-Hammadi, Z. Ren, G. da Silva, Thermal decomposition kinetics of the indenyl radical: a theoretical study, J. Phys. Chem. A 125 (13) (2021) 2782–2790, doi:10.1021/acs.jpca.1c01000.
[179] H. Wang, M. Frenklach, Calculations of rate coefficients for the chemically activated reactions of acetylene with vinylic and aromatic radicals, J. Phys. Chem. 98 (44) (1994) 11465–11489, doi:10.1021/j100095a033.
[180] N.W. Moriarty, N.J. Brown, M. Frenklach, Hydrogen migration in the phenylethen-2-yl radical, J. Phys. Chem. A 103 (35) (1999) 7127–7135, doi:10.1021/jp991481f.
[181] D.S.N. Parker, R.I. Kaiser, T.P. Troy, M. Ahmed, Hydrogen abstraction/acetylene addition revealed, Angew. Chem. Int. Ed. 53 (30) (2014) 7740–7744, doi:10.1002/anie.201404537.
[182] T.-C. Chu, Z.J. Buras, M.C. Smith, A.B. Uwagwu, W.H. Green, From benzene to naphthalene: direct measurement of reactions and intermediates of phenyl radicals and acetylene, Phys. Chem. Chem. Phys. 21 (2019) 22248–22258, doi:10.1039/C9CP04554F.
[183] Q. Mao, L. Shen, H. Pitsch, Reactivity of diacetylene in polycyclic aromatic hydrocarbons growth (Unpublished results).
[184] Q. Mao, L. Pratali Maffei, H. Pitsch, T. Faravelli, Theoretical study of important phenylacetylene reactions in polycyclic aromatic hydrocarbon growth (Unpublished results).
[185] L. Zhao, R.I. Kaiser, W. Lu, B. Xu, M. Ahmed, A.N. Morozov, A.M. Mebel, A.H. Howlader, S.F. Wnuk, Molecular mass growth through ring expansion in polycyclic aromatic hydrocarbons via radical–radical reactions, Nat. Commun. 10 (1) (2019) 1–7.
[186] R.S. Tranter, S.J. Klippenstein, L.B. Harding, B.R. Giri, X. Yang, J.H. Kiefer, Experimental and theoretical investigation of the self-reaction of phenyl radicals, J. Phys. Chem. A 114 (32) (2010) 8240–8261, doi:10.1021/jp1031064.
[187] V.V. Kislov, A.I. Sadovnikov, A.M. Mebel, Formation mechanism of polycyclic aromatic hydrocarbons beyond the second aromatic ring, J. Phys. Chem. A 117 (23) (2013) 4794–4816, doi:10.1021/jp402481y.
[188] L. Zhao, R.I. Kaiser, W. Lu, M. Ahmed, A.D. Oleinikov, V.N. Azyazov, A.M. Mebel, A.H. Howlader, S.F. Wnuk, Gas phase formation of phenalene via 10π-aromatic, resonantly stabilized free radical intermediates, Phys. Chem. Chem. Phys. 22 (2020) 15381–15388, doi:10.1039/D0CP02216K.
[189] L. Zhao, M. Prendergast, R.I. Kaiser, B. Xu, U. Ablikim, W. Lu, M. Ahmed, A.D. Oleinikov, V.N. Azyazov, A.H. Howlader, S.F. Wnuk, A.M. Mebel, How to add a five-membered ring to polycyclic aromatic hydrocarbons (PAHs) – molecular mass growth of the 2-naphthyl radical ($C_{10}H_7$) to benzindenes ($C_{13}H_{10}$) as a case study, Phys. Chem. Chem. Phys. 21 (2019) 16737–16750, doi:10.1039/C9CP02930C.
[190] D.P. Porfiriev, V.N. Azyazov, A.M. Mebel, Conversion of acenaphthalene to phenalene via methylation: a theoretical study, Combust. Flame 213 (2020) 302–313, doi:10.1016/j.combustflame.2019.11.038.
[191] Z.D. Levey, B.A. Laws, S.P. Sundar, K. Nauta, S.H. Kable, G. da Silva, J.F. Stanton, T.W. Schmidt, PAH growth in flames and space: formation of the phenalenyl radical, J. Phys. Chem. A 126 (1) (2022) 101–108, doi:10.1021/acs.jpca.1c08310.
[192] L.B. Tuli, A.M. Mebel, Formation of phenanthrene via H-assisted isomerization of 2-ethynylbiphenyl produced in the reaction of phenyl with phenylacetylene, Int. J. Chem. Kinet. 52 (12) (2020) 875–883, doi:10.1002/kin.21406.
[193] T. Yang, R.I. Kaiser, T.P. Troy, B. Xu, O. Kostko, M. Ahmed, A.M. Mebel, M.V. Zagidullin, V.N. Azyazov, HACA's heritage: a free-radical pathway to phenanthrene in circumstellar envelopes of asymptotic giant branch stars, Angew. Chem. Int. Ed. 56 (16) (2017) 4515–4519, doi:10.1002/anie.201701259.
[194] S.E. Stein, A. Fahr, High-temperature stabilities of hydrocarbons, J. Phys. Chem. 89 (17) (1985) 3714–3725, doi:10.1021/j100263a027.
[195] M. Frenklach, T. Yuan, M.K. Ramachandra, Soot formation in binary hydrocarbon mixtures, Energy Fuels 2 (4) (1988) 462–480, doi:10.1021/ef00010a013.
[196] D. Chen, K. Wang, H. Wang, Violation of collision limit in recently published reaction models, Combust. Flame 186 (2017) 208–210, doi:10.1016/j.combustflame.2017.08.005.
[197] S. Davis, C. Law, H. Wang, An experimental and kinetic modeling study of propyne oxidation, Symp. (Int.) Combust. 27 (1) (1998) 305–312, doi:10.1016/S0082-0784(98)80417-7.
[198] R.G. Butler, I. Glassman, Cyclopentadiene combustion in a plug flow reactor near 1150 K, Proc. Combust. Inst. 32 (1) (2009) 395–402, doi:10.1016/j.proci.2008.05.010.
[199] H. Wang, Z. Liu, S. Gong, Y. Liu, L. Wang, X. Zhang, G. Liu, Experimental and kinetic modeling study on 1,3-cyclopentadiene oxidation and pyrolysis, Combust. Flame 212 (2020) 189–204, doi:10.1016/j.combustflame.2019.10.032.
[200] A. Lovell, K. Brezinsky, I. Glassman, Benzene oxidation perturbed by NO_2 addition, Symp. (Int.) Combust. 22 (1) (1989) 1063–1074, doi:10.1016/S0082-0784(89)80116-X.
[201] H. Ciezki, G. Adomeit, Shock-tube investigation of self-ignition of *n*-heptane-air mixtures under engine relevant conditions, Combust. Flame 93 (4) (1993) 421–433, doi:10.1016/0010-2180(93)90142-P.
[202] R. Minetti, M. Carlier, M. Ribaucour, E. Therssen, L. Sochet, A rapid compression machine investigation of oxidation and auto-ignition of *n*-heptane: measurements and modeling, Combust. Flame 102 (3) (1995) 298–309, doi:10.1016/0010-2180(94)00236-L.
[203] C. Ji, E. Dames, Y.L. Wang, H. Wang, F.N. Egolfopoulos, Propagation and extinction of premixed C_5-C_{12} *n*-alkane flames, Combust. Flame 157 (2) (2010) 277–287, doi:10.1016/j.combustflame.2009.06.011.
[204] S. Jerzembeck, N. Peters, P. Pepiot-Desjardins, H. Pitsch, Laminar burning velocities at high pressure for primary reference fuels and gasoline: experimental and numerical investigation, Combust. Flame 156 (2) (2009) 292–301, doi:10.1016/j.combustflame.2008.11.009.
[205] K. Fieweger, R. Blumenthal, G. Adomeit, Self-ignition of S.I. engine model fuels: a shock tube investigation at high pressure, Combust. Flame 109 (4) (1997) 599–619, doi:10.1016/S0010-2180(97)00049-7.
[206] M. Fikri, J. Herzler, R. Starke, C. Schulz, P. Roth, G. Kalghatgi, Autoignition of gasoline surrogates mixtures at intermediate temperatures and high pressures, Combust. Flame 152 (1) (2008) 276–281, doi:10.1016/j.combustflame.2007.07.010.
[207] P. Dirrenberger, P. Glaude, R. Bounaceur, H. Le Gall, A.P. da Cruz, A. Konnov, F. Battin-Leclerc, Laminar burning velocity of gasolines with addition of ethanol, Fuel 115 (2014) 162–169, doi:10.1016/j.fuel.2013.07.015.

[208] M. Chaos, Z. Zhao, A. Kazakov, P. Gokulakrishnan, M. Angioletti, F.L. Dryer, A PRF + toluene surrogate fuel model for simulating gasoline kinetics, Proceedings of the 5th U.S. National Combustion Meeting (2007).
[209] L. Cancino, M. Fikri, A. Oliveira, C. Schulz, Autoignition of gasoline surrogate mixtures at intermediate temperatures and high pressures: experimental and numerical approaches, Proc. Combust. Inst. 32 (1) (2009) 501–508, doi:10.1016/j.proci.2008.06.180.
[210] B. Chen, P. Liu, Q. Xu, Z. Wang, W.L. Roberts, H. Pitsch, Low temperature oxidation of toluene in an *n*-heptane/toluene mixture, Combust. Flame 242 (2022) 112200, doi:10.1016/j.combustflame.2022.112200.
[211] P. Dagaut, M. Reuillion, M. Cathonnet, High pressure oxidation of liquid fuels from low to high temperature. 2. Mixtures of *n*-heptane and iso-octane, Combust. Sci. Technol. 103 (1–6) (1994) 315–336, doi:10.1080/00102209408907701.
[212] D. Bradley, R. Hicks, M. Lawes, C. Sheppard, R. Woolley, The measurement of laminar burning velocities and Markstein numbers for iso-octane–air and iso-octane–*n*-heptane–air mixtures at elevated temperatures and pressures in an explosion bomb, Combust. Flame 115 (1) (1998) 126–144, doi:10.1016/S0010-2180(97)00349-0.
[213] C.T. Bowman, A shock-tube investigation of the high-temperature oxidation of methanol, Combust. Flame 25 (1975) 343–354, doi:10.1016/0010-2180(75)90106-6.
[214] K.E. Noorani, B. Akih-Kumgeh, J.M. Bergthorson, Comparative high temperature shock tube ignition of C_1–C_4 primary alcohols, Energy Fuels 24 (11) (2010) 5834–5843, doi:10.1021/ef1009692.
[215] K. Natarajan, K. Bhaskaran, An Experimental and Analytical Investigation of High Temperature Ignition of Ethanol, Technical Report, Indian Institute of Technology Madras Dept. of Mechanical Engineering, 1981.
[216] P.S. Veloo, Y.L. Wang, F.N. Egolfopoulos, C.K. Westbrook, A comparative experimental and computational study of methanol, ethanol, and *n*-butanol flames, Combust. Flame 157 (10) (2010) 1989–2004, doi:10.1016/j.combustflame.2010.04.001.
[217] J. Beeckmann, L. Cai, H. Pitsch, Experimental investigation of the laminar burning velocities of methanol, ethanol, *n*-propanol, and *n*-butanol at high pressure, Fuel 117 (2014) 340–350, doi:10.1016/j.fuel.2013.09.025.
[218] D.J. Seery, C.T. Bowman, An experimental and analytical study of methane oxidation behind shock waves, Combust. Flame 14 (1) (1970) 37–47, doi:10.1016/S0010-2180(70)80008-6.
[219] C.M. Vagelopoulos, F.N. Egolfopoulos, Direct experimental determination of laminar flame speeds, Symp. (Int.) Combust. 27 (1) (1998) 513–519, doi:10.1016/S0082-0784(98)80441-4.
[220] M. Hassan, K. Aung, G. Faeth, Measured and predicted properties of laminar premixed methane/air flames at various pressures, Combust. Flame 115 (4) (1998) 539–550, doi:10.1016/S0010-2180(98)00025-X.
[221] G. Rozenchan, D. Zhu, C. Law, S. Tse, Outward propagation, burning velocities, and chemical effects of methane flames up to 60 atm, Proc. Combust. Inst. 29 (2) (2002) 1461–1470, doi:10.1016/S1540-7489(02)80179-1.
[222] K. Bosschaart, L. de Goey, The laminar burning velocity of flames propagating in mixtures of hydrocarbons and air measured with the heat flux method, Combust. Flame 136 (3) (2004) 261–269, doi:10.1016/j.combustflame.2003.10.005.
[223] Y. Hidaka, K. Hattori, T. Okuno, K. Inami, T. Abe, T. Koike, Shock-tube and modeling study of acetylene pyrolysis and oxidation, Combust. Flame 107 (4) (1996) 401–417, doi:10.1016/S0010-2180(96)00094-6.
[224] M. Rickard, J. Hall, E. Petersen, Effect of silane addition on acetylene ignition behind reflected shock waves, Proc. Combust. Inst. 30 (2) (2005) 1915–1923, doi:10.1016/j.proci.2004.08.035.
[225] F. Egolfopoulos, D. Zhu, C. Law, Experimental and numerical determination of laminar flame speeds: mixtures of C_2-hydrocarbons with oxygen and nitrogen, Symp. (Int.) Combust. 23 (1) (1991) 471–478, doi:10.1016/S0082-0784(06)80293-6.
[226] G. Jomaas, X. Zheng, D. Zhu, C. Law, Experimental determination of counterflow ignition temperatures and laminar flame speeds of C_2–C_3 hydrocarbons at atmospheric and elevated pressures, Proc. Combust. Inst. 30 (1) (2005) 193–200, doi:10.1016/j.proci.2004.08.228.
[227] M. Baroncelli, D. Felsmann, N. Hansen, H. Pitsch, Investigating the effect of oxy-fuel combustion and light coal volatiles interaction: a mass spectrometric study, Combust. Flame 204 (2019) 320–330, doi:10.1016/j.combustflame.2019.03.017.
[228] D. Horning, A Study of the High-temperature Autoignition and Thermal Decomposition of Hydrocarbons, Stanford University, Stanford, California, U.S.A., 2001 Ph.D. thesis.
[229] Y. Hidaka, T. Nishimori, K. Sato, Y. Henmi, R. Okuda, K. Inami, T. Higashihara, Shock-tube and modeling study of ethylene pyrolysis and oxidation, Combust. Flame 117 (4) (1999) 755–776, doi:10.1016/S0010-2180(98)00128-X.
[230] F. Carbone, K. Gleason, A. Gomez, Pressure effects on incipiently sooting partially premixed counterflow flames of ethylene, Proc. Combust. Inst. 36 (1) (2017) 1395–1402, doi:10.1016/j.proci.2016.07.041.
[231] T. Hirasawa, C. Sung, A. Joshi, Z. Yang, H. Wang, C. Law, Determination of laminar flame speeds using digital particle image velocimetry: binary fuel blends of ethylene, *n*-butane, and toluene, Proc. Combust. Inst. 29 (2) (2002) 1427–1434, doi:10.1016/S1540-7489(02)80175-4.
[232] K. Kumar, G. Mittal, C.-J. Sung, C.K. Law, An experimental investigation of ethylene/O_2/diluent mixtures: laminar flame speeds with preheat and ignition delays at high pressures, Combust. Flame 153 (3) (2008) 343–354, doi:10.1016/j.combustflame.2007.11.012.
[233] J. de Vries, J.M. Hall, S.L. Simmons, M.J. Rickard, D.M. Kalitan, E.L. Petersen, Ethane ignition and oxidation behind reflected shock waves, Combust. Flame 150 (1) (2007) 137–150, doi:10.1016/j.combustflame.2006.10.008.
[234] H. Curran, J.M. Simmie, P. Dagaut, D. Voisin, M. Cathonnet, The ignition and oxidation of allene and propyne: experiments and kinetic modeling, Symp. (Int.) Combust. 26 (1) (1996) 613–620, doi:10.1016/S0082-0784(96)80267-0.
[235] Z. Qin, H. Yang, W.C. Gardiner, Measurement and modeling of shock-tube ignition delay for propene, Combust. Flame 124 (1) (2001) 246–254, doi:10.1016/S0010-2180(00)00200-5.
[236] K. Saeed, R. Stone, Laminar burning velocities of propene–air mixtures at elevated temperatures and pressures, J. Energy Inst. 80 (2) (2007) 73–82, doi:10.1179/174602207X186916.
[237] C. Brown, G. Thomas, Experimental studies of shock-induced ignition and transition to detonation in ethylene and propane mixtures, Combust. Flame 117 (4) (1999) 861–870, doi:10.1016/S0010-2180(98)00133-3.
[238] A. Burcat, A. Lifshitz, K. Scheller, G.B. Skinner, Shock-tube investigation of ignition in propane-oxygen-argon mixtures, Symp. (Int.) Combust. 13 (1) (1971) 745–755, doi:10.1016/S0082-0784(71)80077-2.
[239] C. Vagelopoulos, F. Egolfopoulos, C. Law, Further considerations on the determination of laminar flame speeds with the counterflow twin-flame technique, Symp. (Int.) Combust. 25 (1) (1994) 1341–1347, doi:10.1016/S0082-0784(06)80776-9.
[240] Y. Li, E. O'Connor, C.-W. Zhou, H.J. Curran, An experimental study of butene isomers and 1,3-butadiene ignition delay times at elevated pressures, Proceedings of the European Combustion Meeting, Budapest, Hungary (2015).
[241] S.G. Davis, C. Law, Determination of and fuel structure effects on laminar flame speeds of C_1 to C_8 hydrocarbons, Combust. Sci. Technol. 140 (1–6) (1998) 427–449, doi:10.1080/00102209808915781.
[242] K. Moshammer, L. Seidel, Y. Wang, H. Selim, S.M. Sarathy, F. Mauss, N. Hansen, Aromatic ring formation in opposed-flow diffusive 1,3-butadiene flames, Proc. Combust. Inst. 36 (1) (2017) 947–955, doi:10.1016/j.proci.2016.09.010.
[243] M. Baroncelli, Q. Mao, H. Pitsch, N. Hansen, Effects of C_1–C_3 hydrocarbon blending on aromatics formation in 1-butene counterflow flames, Combust. Flame 230 (2021) 111427, doi:10.1016/j.combustflame.2021.111427.
[244] J. Orme, H. Curran, J. Simmie, Shock tube study of 5 membered cyclic hydrocarbon oxidation, Proceedings of the European Combustion Meeting, Louvain-la-Neuve, Belgium (2005).
[245] C. Ji, R. Zhao, B. Li, F.N. Egolfopoulos, Propagation and extinction of cyclopentadiene flames, Proc. Combust. Inst. 34 (1) (2013) 787–794, doi:10.1016/j.proci.2012.07.047.
[246] A. Burcat, C. Snyder, T. Brabbs, Ignition Delay Times of Benzene and Toluene with Oxygen in Argon Mixtures, Technical Memorandum, NASA, Lewis Research Center, Cleveland, Ohio, U.S.A., 1986.
[247] I.D. Costa, R. Fournet, F. Billaud, F. Battin-Leclerc, Experimental and modeling study of the oxidation of benzene, Int. J. Chem. Kinet. 35 (10) (2003) 503–524, doi:10.1002/kin.10148.
[248] Y. Chai, L.D. Pfefferle, An experimental study of benzene oxidation at fuel-lean and stoichiometric equivalence ratio conditions, Fuel 77 (4) (1998) 313–320, doi:10.1016/S0016-2361(97)00192-0.
[249] A. Ristori, P. Dagaut, A.E. Bakali, G. Pengloan, M. Cathonnet, Benzene oxidation: experimental results in a JDR and comprehensive kinetic modeling in JSR, shock-tube and flame, Combust. Sci. Technol. 167 (1) (2001) 223–256, doi:10.1080/00102200108952183.
[250] K. Brezinsky, The high-temperature oxidation of aromatic hydrocarbons, Prog. Energy Combust. Sci. 12 (1) (1986) 1–24, doi:10.1016/0360-1285(86)90011-0.
[251] R. Johnston, J. Farrell, Laminar burning velocities and Markstein lengths of aromatics at elevated temperature and pressure, Proc. Combust. Inst. 30 (1) (2005) 217–224, doi:10.1016/j.proci.2004.08.075.
[252] H.-P.S. Shen, M.A. Oehlschlaeger, The autoignition of C_8H_{10} aromatics at moderate temperatures and elevated pressures, Combust. Flame 156 (5) (2009) 1053–1062, doi:10.1016/j.combustflame.2008.11.015.
[253] V. Vasudevan, D. Davidson, R. Hanson, Shock tube measurements of toluene ignition times and OH concentration time histories, Proc. Combust. Inst. 30 (1) (2005) 1155–1163, doi:10.1016/j.proci.2004.07.039.
[254] Y. Zhang, K.P. Somers, M. Mehl, W.J. Pitz, R.F. Cracknell, H.J. Curran, Probing the antagonistic effect of toluene as a component in surrogate fuel models at low temperatures and high pressures. A case study of toluene/dimethyl ether mixtures, Proc. Combust. Inst. 36 (1) (2017) 413–421, doi:10.1016/j.proci.2016.06.190.
[255] S.D. Klotz, K. Brezinsky, I. Glassman, Modeling the combustion of toluene-butane blends, Symp. (Int.) Combust. 27 (1) (1998) 337–344, doi:10.1016/S0082-0784(98)80421-9.
[256] U. Pfahl, K. Fieweger, G. Adomeit, Self-ignition of diesel-relevant hydrocarbon-air mixtures under engine conditions, Symp. (Int.) Combust. 26 (1) (1996) 781–789, doi:10.1016/S0082-0784(96)80287-6.
[257] K. Mati, A. Ristori, G. Pengloan, P. Dagaut, Oxidation of 1-methylnaphtalene at 1–13 atm: experimental study in a JSR and detailed chemical kinetic modeling, Combust. Sci. Technol. 179 (7) (2007) 1261–1285, doi:10.1080/00102200601146536.
[258] H.-P.S. Shen, J. Vanderover, M.A. Oehlschlaeger, A shock tube study of the auto-ignition of toluene/air mixtures at high pressures, Proc. Combust. Inst. 32 (1) (2009) 165–172, doi:10.1016/j.proci.2008.05.004.
[259] X. Meng, E. Hu, X. Li, Z. Huang, Experimental and kinetic study on laminar flame speeds of styrene and ethylbenzene, Fuel 185 (2016) 916–924, doi:10.1016/j.fuel.2016.08.019.

[260] M. Mehl, O. Herbinet, P. Dirrenberger, R. Bounaceur, P.-A. Glaude, F. Battin-Leclerc, W.J. Pitz, Experimental and modeling study of burning velocities for alkyl aromatic components relevant to diesel fuels, Proc. Combust. Inst. 35 (1) (2015) 341–348, doi:10.1016/j.proci.2014.06.064.
[261] F. Battin-Leclerc, R. Bounaceur, N. Belmekki, P.A. Glaude, Experimental and modeling study of the oxidation of xylenes, Int. J. Chem. Kinet. 38 (4) (2006) 284–302, doi:10.1002/kin.20160.
[262] S. Gaïl, P. Dagaut, G. Black, J.M. Simmie, Kinetics of 1,2-dimethylbenzene oxidation and ignition: experimental and detailed chemical kinetic modeling, Combust. Sci. Technol. 180 (10–11) (2008) 1748–1771, doi:10.1080/00102200802258270.
[263] S. Gaïl, Kinetic Study of the Oxidation of Aromatic Compounds in Relation with S.I. and Diesel Fuels Combustion: Experimental Approach and Detailed Kinetic Modeling Study; Etude Cinetique de l'Oxydation de Composes Aromatiques en Relation avec la Combustion du Gazole et de l'Essence: Approche Experimentale et Modelisation Cinetique Detaillee, University of Orléans, Orléans, France, 2003 Ph.D. thesis.
[264] J.L. Emdee, K. Brezinsky, I. Glassman, High-temperature oxidation mechanisms of *m*- and *p*-xylene, J. Phys. Chem. 95 (4) (1991) 1626–1635, doi:10.1021/j100157a024.
[265] C. Ji, A. Moheet, Y. Wang, M. Colket, H. Wang, F. Egolfopoulos, An experimental study of premixed *m*-xylene/air and *n*-dodecane/*m*-xylene/air flames, Proceedings of the 6th U.S. National Combustion Meeting (2009).
[266] A. Comandini, G. Pengloan, S. Abid, N. Chaumeix, Experimental and modeling study of styrene oxidation in spherical reactor and shock tube, Combust. Flame 173 (2016) 425–440, doi:10.1016/j.combustflame.2016.08.026.
[267] W.L. Oberkampf, M.F. Barone, Measures of agreement between computation and experiment: validation metrics, J. Comput. Phys. 217 (1) (2006) 5–36, doi:10.1016/j.jcp.2006.03.037.
[268] J. Devore, Probability and Statistics for Engineering and the Sciences, Brooks/Cole Publishing Company, Boston, U.S.A., 1987.
[269] M. Frenklach, J. Warnatz, Detailed modeling of PAH profiles in a sooting low-pressure acetylene flame, Combust. Sci. Technol. 51 (4–6) (1987) 265–283, doi:10.1080/00102208708960325.
[270] V. Kislov, R. Singh, D. Edwards, A. Mebel, M. Frenklach, Rate coefficients and product branching ratios for the oxidation of phenyl and naphthyl radicals: a theoretical RRKM-ME study, Proc. Combust. Inst. 35 (2) (2015) 1861–1869, doi:10.1016/j.proci.2014.06.135.
[271] S.J. Klippenstein, L.B. Harding, Y. Georgievskii, On the formation and decomposition of C_7H_8, Proc. Combust. Inst. 31 (1) (2007) 221–229, doi:10.1016/j.proci.2006.08.045.